Ratcheting Fatigue Behaviour and Post-fatigue Tensile Properties of Commercial Aluminium

A thesis submitted in partial fulfillment of the requirement for the degree of

Master of Technology
in
Metallurgical and Materials Engineering

Submitted by

Preeti Verma

Roll No. 209MM1245

Department of Metallurgical and Materials Engineering
National Institute of Technology,
Rourkela-769008

2011

Ratcheting Fatigue Behaviour and Post-fatigue Tensile Properties of Commercial Aluminium

A thesis submitted in partial fulfillment of the requirement for the award of degree of

Master of Technology
in
Metallurgical and Materials Engineering

Submitted by

Preeti Verma

Roll No. 209MM1245

Under the Supervision Of

Prof. K. Dutta

Department of Metallurgical and Materials Engineering
National Institute of Technology,
Rourkela-769008

2011

National Institute of Technology, Rourkela

Certificate

This is to certify that the thesis entitled ***"Ratcheting fatigue behaviour and post-fatigue tensile properties of commercial aluminium"*** submitted by Miss. Preeti Verma in partial fulfillment of the requirements for the award of the degree of Master of Technology in Metallurgical and Materials Engineering at National Institute of Technology, Rourkela is an authentic work carried out by her under my supervision and guidance.

To the best of my knowledge, the matter embodied in the thesis has not been submitted to any other university/institute for the award of any degree or diploma.

Date:

Place: Rourkela

Supervisor
Prof. K. Dutta
Department of Metallurgical and Materials Engineering
National Institute of Technology, Rourkela-769008

Acknowledgement

With deep regards and profound respect, I avail this opportunity to express my deep sense of gratitude and indebtedness to Prof. K. Dutta, Metallurgical and Materials Engineering Department, NIT Rourkela, for introducing the present research topic and for his inspiring guidance, constructive criticism and valuable suggestion throughout the research work. It would have not been possible for me to bring out this thesis without his help and constant encouragement.

I am sincerely thankful to Dr B. B. Verma, Professor and Head Metallurgical and Materials Engineering Department and other faculty members of this department for their persistent support and advice during the course work.

I am also highly grateful to laboratory members of Department of Metallurgical and Materials Engineering, NIT Rourkela, specially Mr. Hembram, Mr. R. Pattanaik, and Mr. U. K. Sahu for their help during the execution of experiment.

Last but not the least, I wish to place my deep sense of thanks to my friends for their cooperation and critical suggestion during my project work and studies.

Place: Rourkela **Preeti Verma**

Contents

Abstract

This investigation examines the ratcheting fatigue behaviour and post-fatigue tensile properties of commercial aluminium in annealed and normalised condition. Ratcheting is the phenomena of progressive accumulation of permanent deformation when a component is subjected to asymmetric cyclic loading which also causes variation in their mechanical properties. One set of commercial aluminium rods were annealed by soaking the as received rods at 200°C for 30 minutes prior to machining and other set were normalised up to same temperature with same soaking time. The microstructural examinations were carried out with the help of optical microscope as well as by scanning electron microscope. Hardness measurements were done using a Vickers hardness tester by applying 3kg load with dwell time of 15 s.

Specimen for fatigue test were designed with test section diameter of 10mm and reduced gauge length of 20mm. stress controlled fatigue test were carried out at room temperature up to 150 cycle under different combination of mean stress and stress amplitude in servo-hydraulic testing machine. In annealed condition mean stress is 40, 45, 50 MPa and stress amplitude is 175, 185 MPa, while in normalised condition mean stress is 30, 35, 40 MPa and stress amplitude is 170, 180 MPa. Fatigue test were done at a constant stress rate of 50 MPa/s. In addition a series of specimens were first subjected to 150 cycles of loading prior to carrying out tensile test on these specimens using nominal strain rate 0.83×10^{-5} s^{-1}. Fractographic studies were carried out on the broken samples by using SEM. Hardness was measured after post-fatigue tensile test.

The results highlight that accumulation of ratcheting strain increases with increasing mean stress and stress amplitude in both annealed and normalised condition. In normalised condition strain accumulation is less in comparison to annealed. Strain accumulation get saturated after about 40 cycles in annealed condition and 30 cycles in normalised condition for any of the selected test parameters. Post-fatigue tensile strength increases with mean stress and stress amplitude but with associated reduced ductility. It is observed that dimple size decreases with increase in strain accumulation. Hardness also increases with increase in strain accumulation. The increase in strain accumulation is explained by the phenomenon of increased dislocation density during asymmetric cyclic loading, whereas the increase in tensile strength and decrease in ductility are attributed to cyclic hardening.

Key words: Mean stress, stress amplitude, ratcheting strain, post-fatigue tensile properties.

List of Figures

List of Tables

CHAPTER - 1

INTRODUCTION

1.0 Introduction

Aluminium and its alloys are candidate materials for application in many industries like automobile and aerospace sectors, due to their high strength to weight ratio. This helps in moving a vehicle made up with aluminium or aluminium alloys using lower energy, as it is known from Newton's second law of motion that less force is required to move lighter objects. It is also remarkable for its ability to resist corrosion. Aluminium alloys continue to be dominating structural material for aircraft. The cost reduction for aircraft has become an important criterion in many airlines. In addition to that, selection of material is also done on the basis of life cycle approach. The composites are very competitive materials for aircraft structural application. However they are generally considered to have higher initial cost, require more manual labour in their production and more expensive to maintain. It is known that almost 90% of every service failure occurs due to fatigue and it is reported that the nature of fatigue failure greatly depends upon the nature of loading [1]. The fatigue life of materials may vary to a great extent when the cyclic loading behaviour changes. Symmetric strain cycling in the plastic range termed as LCF and asymmetric stress cycling is termed as ratcheting [2]. Ratcheting is the phenomena of progressive accumulation of permanent deformation when a component is subjected to asymmetric cyclic loading [3]. On the other hand it can also be defined as accumulation of plastic strain with the application of cyclic loading characterized by a non-zero mean stress. After a sufficient number of cycles the total strain (displacement) become so large that the original shape of the structure is altered, thereby making the structure unserviceable. It is one of the important factors that should be considered in the design of structural components. It can be potentially deleterious because for a suitable combination of mean stress (σ_m) and stress amplitude (σ_a), continuous accumulation of plastic strain may take place in every cycle. The study of strain accumulation due to asymmetrical stress cycling in structural materials for piping application has been the subject of investigations in recent years [4-6].

Most of the materials display a cyclic hardening/softening behaviour. Some materials such as the stainless steel and pure copper, exhibit very significant cyclic hardening while some other material such as 1070 steel display less significant effect on hardening or softening [2,3,7]. The materials like CS1026, SA333Gr6, 25CDV4.11 and 9Mo-1Cr exhibit cyclic softening feature [3-4,8-9,] In general a hard material (cold worked,

quenched) cyclically softens and a soft material (annealed) cyclically hardens [3,10]. Therefore, it would be interesting and of great scientific requirement to develop an understanding of the post-ratcheting mechanical properties and variations in material micro-mechanism.

In the last two decades, many experimental results of uniaxial and multiaxial ratcheting for SS304 and 316FR stainless steels are proposed by some researchers. A review of the existing results reflects the fact that ratcheting behaviour depends on type of material, cyclic softening/hardening behaviours of materials as well as their loading history [5,11-14]

Although literature is available on fatigue performance of aluminium under low cycle or high cycle fatigue conditions, yet some comparative assessment of fatigue performance and related variations in mechanical properties in post-fatigue conditions will give some value-addition to the literature. The low cycle fatigue test for the materials were conducted generally under strain controlled cyclic loading, while enough attention was not paid to stress controlled low cycle fatigue test. Here we will do experiment for low cycle fatigue test of aluminium under stress control.

1.1 Objectives of the present work

1. To characterize the material that is to be tested.
2. To study the effects of loading conditions on accumulation of ratcheting strain of aluminium in annealed and normalised conditions.
3. To study the post-fatigue tensile properties of cyclically damaged samples.
4. Fractographic study of broken specimens.
5. To determine the hardness of post-fatigue tensile specimens.

1.2 Lay out of the work

The thesis is divided into six chapters, the contents of which are discussed in brief as follows:

Chapter 1 presents a general background dealing with the emergence of aluminium as class of lightweight materials for use in automotive and aerospace structural

components, scientific issues pertaining to relevant structure-property relations with emphasis on ratcheting behaviour, and motivation to pursue the present work. An overview of the objectives and scope of the present work is also presented in this chapter.

Chapter 2 provides a critical review of the existing literature related to the effect of mean stress, stress amplitude, cyclic hardening/softening and type of loading and material on ratcheting behaviour with an objective to analyze the controversies and unresolved issues. The information in the published literature raises unanswered questions and provides the directions for further research. The present study has been inspired by the achievements of the previous investigations.

Chapter 3 comprise a detailed description of the experiments which have been conducted during this investigation. The experiments include (i) chemical composition analysis, (ii) characterization of microstructures, (iii) hardness and tensile test, (iv) fatigue test, (iv) post-fatigue tensile test and (v) fracture surface examination using scanning electron microscope (SEM).

Chapter 4 presents a comparative study of the microstructure, hardness tensile properties of annealed and normalised aluminium. The effects of stress amplitude and mean stress on ratcheting strain and post-fatigue tensile properties have been discussed. Variation in the fracture signatures on the fracture surface with varying loading conditions is also discussed.

Chapter 5 presents the summary and the major conclusions drawn from the present work and future work. Critical analyses of the results provide ideas and directions for further investigation, which have also been discussed in this chapter.

Chapter 6 presents references.

CHAPTER - 2

LITERATURE REVIEW

2.0 Fatigue

When a component is subjected to fluctuating stresses, it may fail at stress levels much lower than its monotonic fracture strength [1]. The underlying failure process involves a gradual cracking of the component and is called Fatigue. Fatigue has become progressively more relevant in developed technology in the areas, such as automobiles, aircraft, compressors, pumps, turbines, etc., that are subjected to repeated loading and vibration. Today it is often stated that fatigue accounts for at least 90 percent of all service failures due to mechanical causes. Three basic factors are necessary to cause fatigue failure. These are:

- maximum tensile stresses of sufficiently high value,
- large enough variation or fluctuation in the applied stress, and
- Sufficiently large number of cycles of the applied stress.

In addition, there are a host of other variables, such as stress concentration, corrosion, temperature, overload, metallurgical structure, residual stresses, and combined stresses, which tend to alter the conditions for fatigue.

Although fatigue failures may seem to be abrupt, the process of fatigue fracture is progressive, beginning as minture cracks that grow during the service life of components. Sub-microscopic changes take place in the crystalline structure of metals and alloys under the action of repetitive low-level load applications. These minute changes accumulate to lead to the formation of tiny microscopic cracks. The tiny cracks grow under cyclic loading into larger cracks. The larger cracks continue to grow until the stress in the remaining ligament becomes unsustainable, when sudden failure occurs. The growth history of fatigue cracks can conveniently be sub-divided into three stages: Crack Initiation, Incremental Crack Growth and Final Fracture.

2.1 Stress Cycles

General types of fluctuating stress which can cause fatigue are given below:

Figure 2.1(a) illustrates completely reversed cycle of stress of sinusoidal form. For this type of stress cycle the maximum and minimum stresses are equal. In other words we can

say symmetric loading ($\sigma_m = 0$). Tensile stress is considered positive and compressive stress is negative.

Figure 2.1(b) illustrates a repeated stress cycle in which the maximum stress σ_{max} and σ_{min} are not equal. In this illustration both are in tension, but a repeated stress cycle could just as well contain maximum and minimum stresses of opposite signs or both in tension. This is known as asymmetric loading ($\sigma_m \neq 0$).

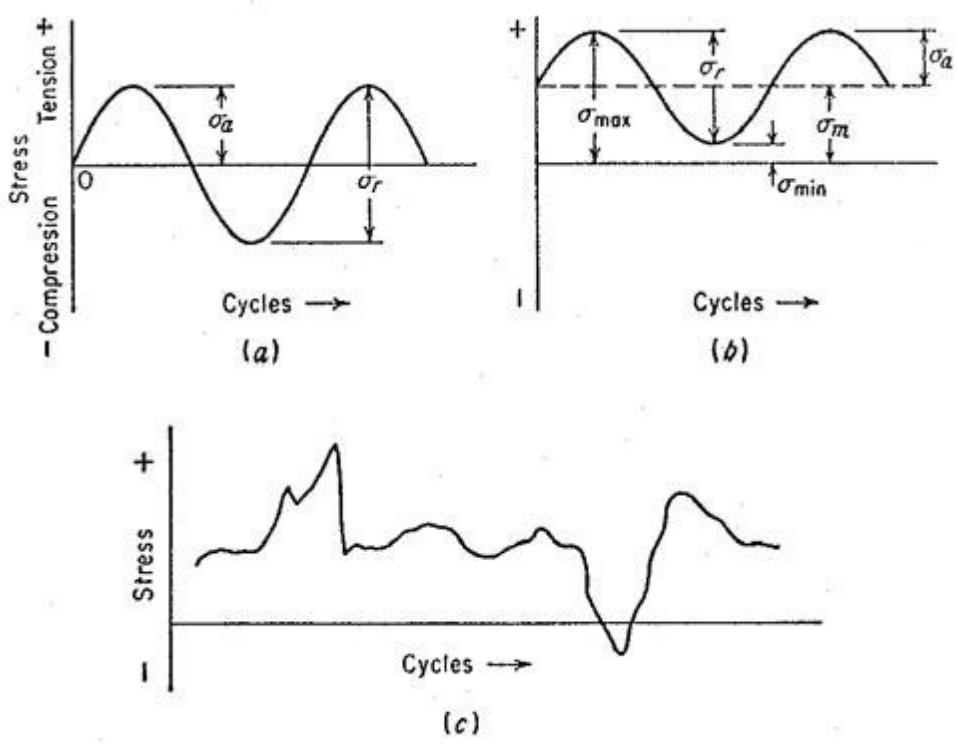

Fig. 2.1: (a) reversed stress cycle (b) repeated stress cycle (c) irregular or random stress cycle.

Figure 2.1(c) illustrates a complicated stress cycle which might be encountered in a part such as an aircraft wing which is subjected to periodic unpredictable load due to gusts.

2.2 The S-N Curve

The basic method of presenting engineering fatigue data is by means of the S-N curve Figure 2.2, a plot of stress against the number of cycles to failure N. A log scale is almost always used for N. The value of stress that is plotted can be stress amplitude (σ_a), maximum stress (σ_{max}), or minimum stress

(σ_{min}). The stress values are usually nominal stresses, i.e., there is no adjustment for stress concentration. The S-N relationship is determined for a specified value of σ_m, stress ratio ($R = \sigma_{min}/\sigma_{max}$), or amplitude ratio ($A = \sigma_a/\sigma_m$).

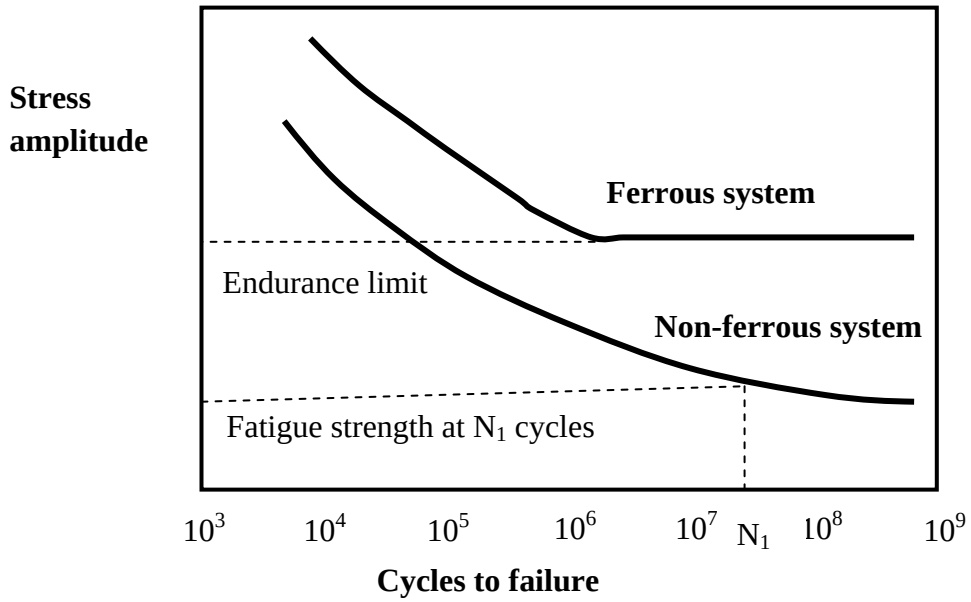

Fig. 2.2: Schematic representation of S-N curve: (A) Ferrous system; (B) Non-ferrous system.

For determinations of the S-N curve, the usual procedure is to test the first specimen at a high stress where failure is expected in a fairly short number of cycles, e.g., at about two-thirds the static tensile strength of the material. The test stress is decreased for each succeeding specimen until one or two specimens do not fail in the specified numbers of cycles, which is usually at least 10^7 cycles. This method is used for presenting fatigue failure in high cycles ($N > 10^5$). In high cycle fatigue test stress level is relatively low and the deformation is in elastic range.

For a few important engineering materials such as steel and titanium, the S-N curve becomes horizontal at a certain limiting stress. Below this limiting stress, which is called the fatigue limit, or endurance limit, the material presumably can endure an infinite number of cycles without failures. Most nonferrous metals, like aluminium, magnesium, and copper alloys, have an S-N curve which slopes gradually downward with increasing number of cycles. These materials do not have a true fatigue limit because the S-N curve

never becomes horizontal.

The highest stress at which a non-failure is obtained is taken as the fatigue limit. For materials without a fatigue limit the test is usually terminated for practical considerations at a low stress where the life is about 10^8 or $5x10^8$ cycles. The S-N curve is usually determined with about 8 to 12 specimens.

This curve is used to predict the number of cycles sustained under certain stress before failure. The curve gives designers a quick reference of the allowable stress level for an intended service life.

2.3 High Cycle Fatigue and Low Cycle Fatigue

Fatigue failure can be divided into two forms encompassing the total life of a component, low and high cycle fatigue (LCF and HCF).

2.3.1 HCF

In HCF, the life is usually characterized as a function of the stress range applied, and the components fail after a high numbers (Usually higher than 10^6 cycles) of cycles at a relatively low stress (Usually less than 30 % of yield stress), and the deformation experienced is primarily elastic. High cycle fatigue must be consider during design of automobiles, aircraft, compressors, pumps, turbines, etc where vibration occur. HCF test is done at frequency always greater than 1 KHz. The S-N curve in the high cycle region is sometimes described by the Basquin equation

$$N\sigma_a^p = C \qquad \text{..... (1)}$$

Where σ_a is the stress amplitude and p and c are empirical constants.

From physical point of view, the repeated variation of elastic stress in metals induces micro-internal stress above the local yield stress, with dissipation of energy via micro-plastic strain which arrest certain slips due to the increase of dislocations nodes. There is formation of permanent micro-slip bands and de-cohesions, often at the surface of the material, to produce the mechanism of intrusion extrusion. After this stage crack located inside grain where the micro cracks follow the plane of maximum shear stress. In next

stage in which the micro cracks crosses the grain boundary and grow more or less perpendicular to the direction of principal stress up to coalescence to produce a messo-crack.

2.3.2 LCF

The opposite applies for LCF, where life is nominally characterized as a function of the strain range and the component fails after a small number of cycles at a high stress, and the deformation is largely plastic. Strain controlled cyclic loading is found in thermal cycling, where a component expands and contracts in response to fluctuations in the operating temperature. Low cycle fatigue must be considered during design of nuclear pressure vessels, steam turbines and other type of power machineries. Low cycle fatigue test is done at frequency less than 1 Hz.

The usual way of presenting low-cycle fatigue test results is to plot the plastic strain range $\Delta\varepsilon_p$ against N. This graph is plotted in log-log coordinates is shown in Figure 2.3.

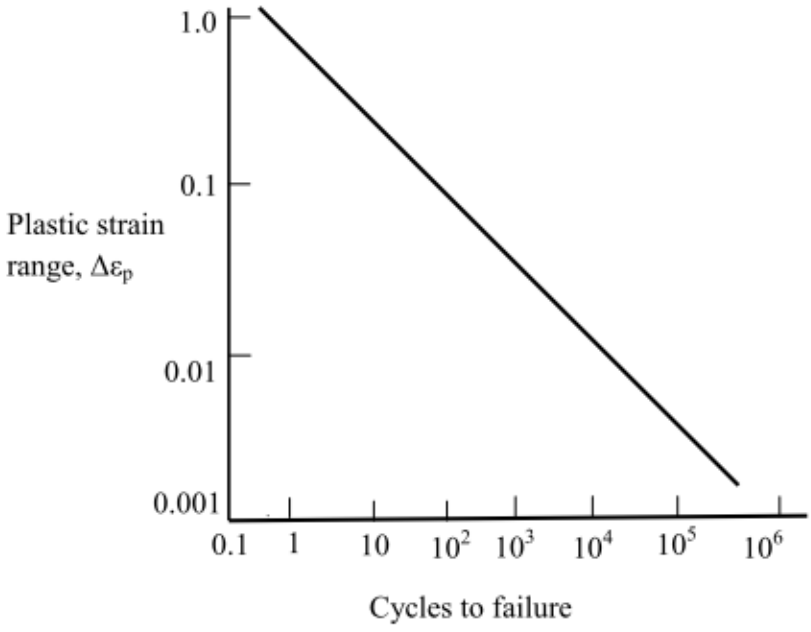

Fig. 2.3: Low cycle fatigue curve.

This type of behaviour is known as the Coffin-Manson relation, which is described by

$$\frac{\Delta\varepsilon_p}{2} = \varepsilon_f'(2N)^C \quad \text{..... (2)}$$

Where,

$\Delta\varepsilon_p/2$ = plastic strain amplitude

ε_f' = fatigue ductility coefficient defined by strain intercept at 2N = 1

2N = number of strain reversals to failure

C = fatigue ductility exponent, which varies between -0.5 and -0.7 for many metals.

2.4 Effect of mean stress on fatigue

Much of the fatigue data in the literature have been determined for conditions of completely reversed cycles of stress, $\sigma_m = 0$. However, conditions are frequently met in engineering practice where the stress situation consists of an alternating stress and a superimposed mean, or steady, stress. There are several possible methods of determining an S-N diagram for a situation where the mean stress is not equal to zero. Figure 2.4 shows the formulations that are used to take account of mean stress in describing the fatigue endurance limit. In general, all these relationships show that with increase of mean stress the alternating stress amplitude required for fatigue endurance limit gradually decreases.

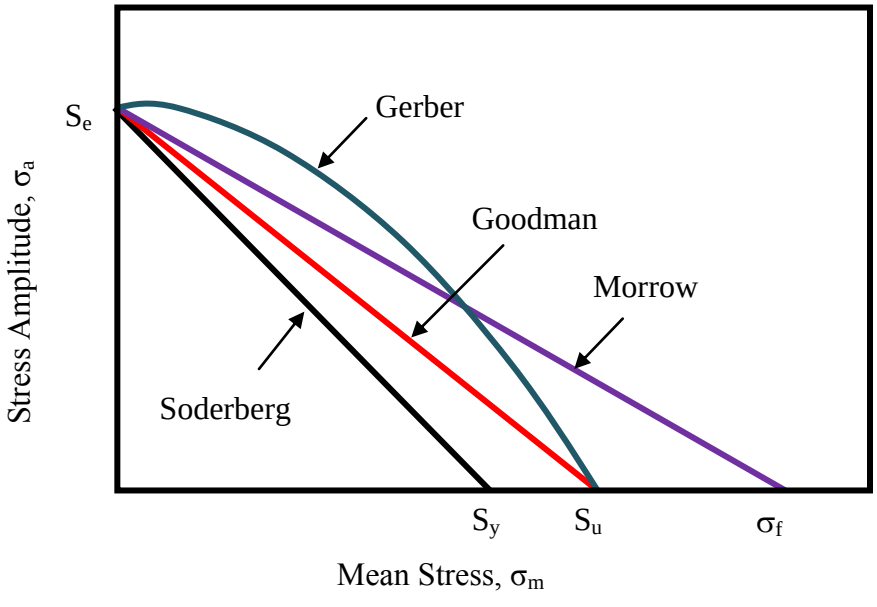

Fig. 2.4: Effect of mean stress on alternating stress amplitude at fatigue endurance.

The mathematical formulations for the various curves in Figure 2.4 are:

Morrow: $(\sigma_a/\sigma_e) + (\sigma_m/\sigma_f) = 1$ ..... (3)

Gerber: $(\sigma_a/\sigma_e) + (\sigma_m/\sigma_u)^2 = 1$ ..... (4)

Goodman: $(\sigma_a/\sigma_e) + (\sigma_m/\sigma_u) = 1$ ..... (5)

Soderberg: $(\sigma_a/\sigma_e) + (\sigma_m/\sigma_y) = 1$ ..... (6)

The Goodman relation gives good result for brittle materials and conservative results for ductile materials. The Gerber relation will give good results for ductile material. Fatigue strength of a component tends to increase with a compressive mean stress and decrease with a tensile mean stress. Gerber's parabolic relationship may therefore yield erroneous answer to the conservative side in the compressive mean stress region.

2.5 Different approaches to fatigue life prediction

2.5.1 Stress based approach

The very first systematic study of metal fatigue using the stress based approach was by Wohler (1871) on rotating axles [15]. Since Wohler 1871 work, fatigue data have been presented in the form of S-N curve. A similar relation Basquin (1910) was proposed. True stress amplitude $\sigma_a = \Delta\sigma/2$ is used as the damage parameter instead of engineering stress

Basquin Relationship is

$\sigma_a = \sigma_f (2N_f)^b$ ..... (7)

Where, σ_f and b are the fatigue strength coefficient and the fatigue strength exponent.

The fatigue strength coefficient σ_f may be estimated from the monotonic tension test by setting $\sigma_f \approx \sigma_{f.}$ fatigue strength exponent b, varies from -0.05 to -0.15. Also fatigue strength exponent b, can be calculated from strain hardening exponent n. Stress amplitude-fatigue life behaviour of ASTM A-516 Gr. 70 low alloy carbon steel has been studied [16].

$$b = \frac{-n}{1+5n}$$ ..... (8)

If we take account the effect of mean stress then Basquin Relation will be

$$\sigma_a = (\sigma_f - \sigma_m)(2N_f)^b$$ ..... (9)

Where, σ_m is the mean stress.

The effect of the tensile mean stress is thus equivalent to a reduction of fatigue strength coefficient, and a compressive mean stress has the reverse effect. Combination of mean stress and stress amplitude may result in cyclic dependent creep (ratcheting) strain which lead to a premature creep-fatigue fracture. Stress based approach is mostly applicable to the high cycle fatigue region where the strain are essentially elastic.

2.5.2 Strain based approach:

Strain based approach essentially use the observed trend of the stress approach, i.e. a linear log-log relation between elastic or plastic strain amplitude and fatigue life is employed. The strain based approach was essentially introduced for thermal and low cycle fatigue. It is now very popular method to fatigue life estimation. Coffin-Manson equation can be written as:

$$\frac{\Delta\varepsilon_p}{2} = \varepsilon_f'(2N)^c$$ ..... (10)

Where,

$\Delta\varepsilon_p/2$ = plastic strain amplitude

ε_f' = fatigue ductility coefficient defined by strain intercept at 2N = 1

2N = number of strain reversals to failure

C = fatigue ductility exponent, which varies between -0.5 and -0.7 for many metals.

The mean strain effect in the low cycle fatigue can be accounted for by modifying the Coffin-Manson equation as

$\Delta\varepsilon_p/2 = (\varepsilon_f - \varepsilon_m).(2N_f)^c$ ..... (11)

Where, ε_m is the mean strain.

Under condition of strain cycling cyclic life in terms of reversals to failure is expressed by Coffin-Manson and Basquin relationship

$\Delta\varepsilon_t/2 = \Delta\varepsilon_e/2 + \Delta\varepsilon_p/2 = (\sigma_f/E).(2N_f)^b + (\varepsilon_f).(2N_f)^c$.

Figure 2.5 shows the strain-life plots according to the above relationship. From this equation it is possible to determine the transition life ($2N_t$) and also the transition strain for the changeover between HCF and LCF. It is found from Figure 2.5 that while below transition life plastic strain component predominates and above transition life elastic strain component predominates.

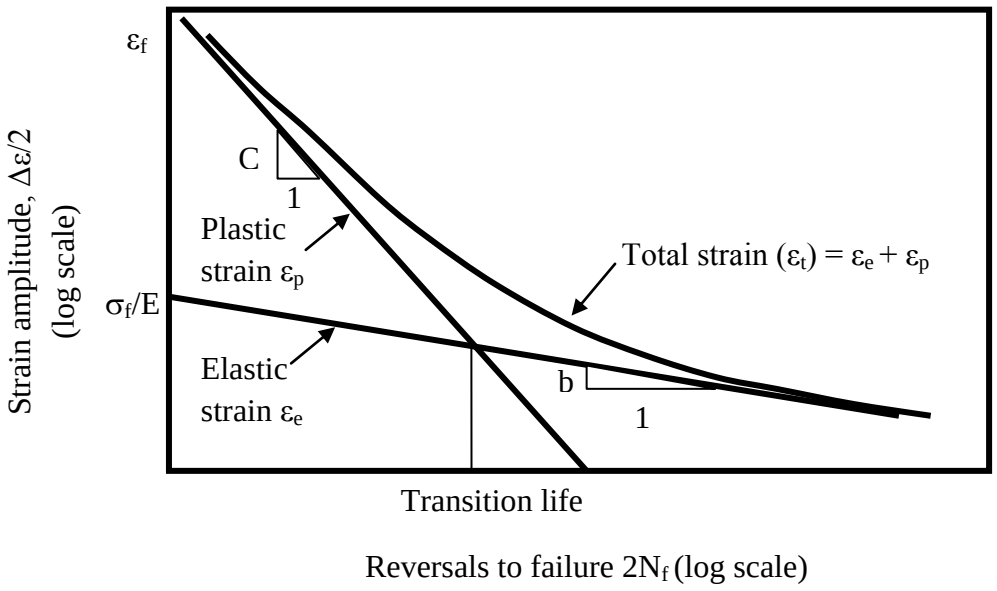

Fig. 2.5: Coffin-Manson and Basquin Plot.

2.6 Monotonic behaviour under tension or compression

The stress-strain relationship of materials in multiaxial stress states has generally been an extension of the observations made in uniaxial tension or compression test. A study of material response under simple tension or compression is therefore an important step in the process of understanding the mechanism of material response.

When a smooth specimen of a circular cross-section with a uniform gauge length is subjected to a slowly increasing load, we can measure the change in length of the uniform section with an extensometer instead of plotting load versus corresponding displacement, it is more useful to choose quantities which render the results independent the specimen geometry.

The uniaxial stress-strain curve for a typical strain hardening material is shown in Figure 2.6 [17]. After loading up to point A, the specimen was unloaded and then reloaded. For small values of the applied load, the response is linear, and the process is reversible between O and A in Figure 2.6, point A being the limit of the elastic response. As the load is increased beyond this limit, permanent deformation set in with the resulting plastic strain. On increasing the load it deviates from the linear response entering an irreversible domain. Two important observations are obtained from this, (i) Following the reloading curve does not pass through the unloading point.(ii) Following the unloading path, the materials yield at point C, at which stress level is higher than the

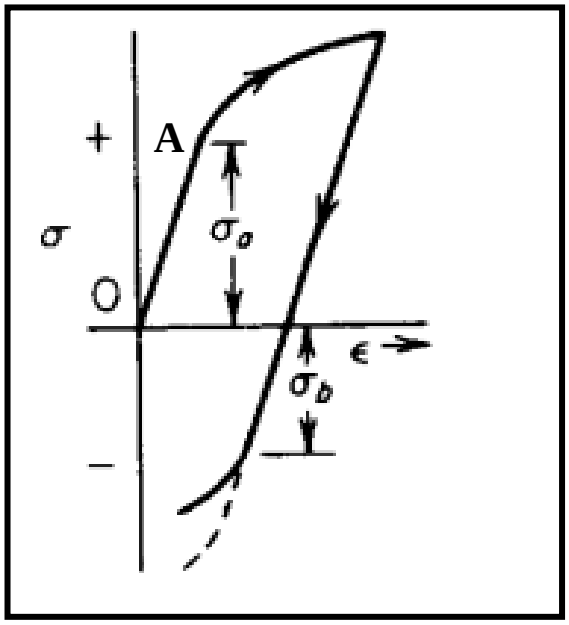

Fig. 2.6: Bauschinger effect.

original compressive yield stress level. The latter observation is known as Bauschinger effect and it indicates that after initial loading over elastic limit, the material property become anisotropic, particularly in the yield stress point. This phenomenon is attributed to the existence of internal back stresses which facilitate the dislocation motion during load reversal. It should be noted that most of the inelastic deformation of crystalline material takes place by glide and climb motion of dislocations. The kinetics of the motion of dislocation in a slip plane will depend on the current state of many obstacles, thereby producing an easily reversed plastic deformation.

The loop traced by the unloading and reloading is called a hysteresis loop, and it is indicative of the absorbed plastic strain energy during the process. The majority of the irrecoverable energy is converted into heat, and internal damping absorbs a part of it.

In describing the stress-strain curve, we implicitly assumed that response was rate insensitive. A study of dislocation structure will indicate that the rate of strain hardening depends on the current obstacle state of the material (glide resistance or hardness). In addition, of rate of strain hardening would depend on the strain-rate.

In the case of rate sensitive material e.g. austenitic stainless steels and titanium alloys, the stress-strain curve will depend on the chosen control variable (stress or strain) and its rate of application. D. Kujawski et. al [18] observed that the material response to the change in the rate and direction is instantaneous for the strain-controlled test, whereas in the case of the stress controlled test, the response is gradual. Also the transition from elastic to the inelastic deformation is more gradual for the stress-controlled test. However, at room temperature and small strain rates (quasi-static loading), the rate effect may be neglected.

2.7 Material Response to cyclic deformation or loading – transient behaviour

Material response deviates from that of the monotonic, once a reversed plastic deformation takes place. When a smooth solid specimen is subjected to one of the loading programme shown in Figure 2.7, the response will differ depending upon the mode of controlled variable. The essential characteristics include cyclic hardening or softening, cyclic mean stress relaxation, cyclic creep deformation (defined as ratcheting in the current investigation), rate dependency and memory effect.

In the case of fully-reversed strain controlled tests, the material response initially varies with the number of cycles and later stabilizes. D. Lefebvre et.al studied the stress-strain response of pearlitic-ferritic steel (ASTM A-516 Gr. 70) [16]. It indicates strain-softening phenomena, i.e. the uncontrolled stress decreases with increasing number of cycles until a saturated state is achieved. It should be noted that at higher strain range ranges this steel hardens, i.e. uncontrolled stress increases with increasing number of

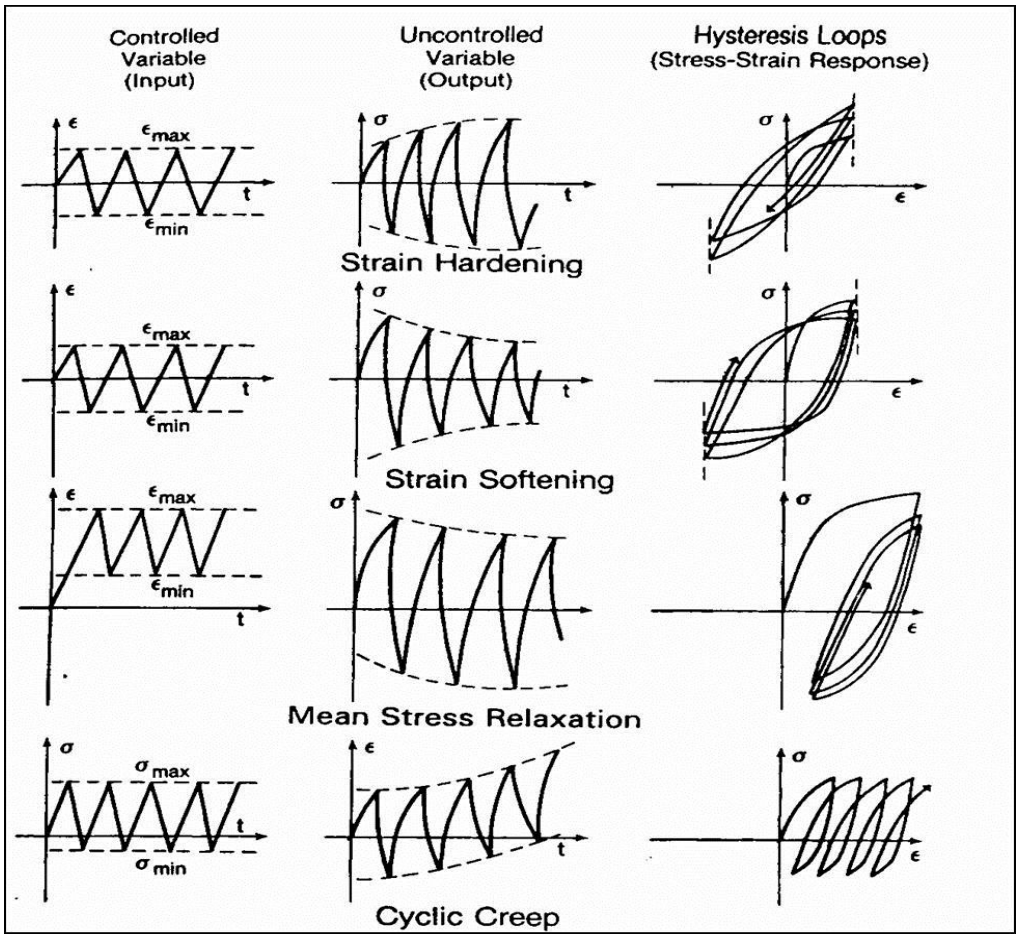

Fig. 2.7: Schematic response to various modes of cyclic input variables (deformation or stress controlled tests) [17].

cycles until it reaches a stable state. This type of behaviour is commonly observed for the low alloy carbon steels. During cyclic deformation the mobile segment of dislocation is reduced, leading to the formation of different obstacle structure. The resistance to dislocation glide is generally increased, thus requiring higher stresses to continue the deformation. The cyclic hardening rate is smaller at low strain amplitudes than at higher ones. For fully-reversed stress-controlled loading, it observes that strain hardening or softening similar to the strain-controlled condition. The plastic strain decreases with the

number of cycles and reaches stable state for strain hardening material. The reverse occurs for strain softening material. When a mean stress is present, the response is rather complicated. For example, in the case of tensile mean stress, creep is observed under stress controlled condition which is shown above in Figure 2.7. The ratcheting strain (cyclic creep strain) increases with increasing number of cycles

It has been seen that the cyclic stress-strain curve differs from that of the monotonic curve in several aspects. First there is transition accompanied by either strain softening or hardening with respect to monotonic curve. A saturated state is subsequently reached. However the transient response depends on the test control mode, i.e. deformation (strain) or load (stress) control, and prior history of deformation.

2.8 Ratcheting

Ratcheting, one of the stress controlled low cycle fatigue responses, is defined as the accumulation of plastic strain with cycles. In other words ratcheting, a strain accumulation under stress controlled cycling with non-zero mean stress, is a predominant phenomenon in cyclic plasticity [19]. This phenomenon is characterized by a translation of the hysteresis loop under non-symmetrical stress loading which is shown in Figure 2.8.

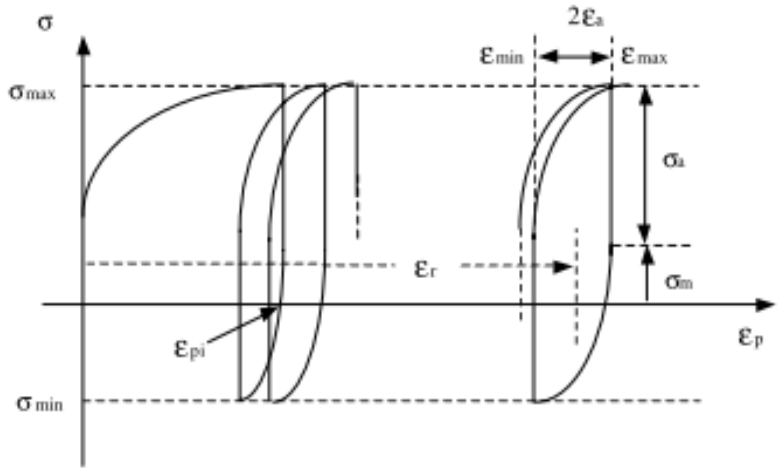

Fig. 2.8: Schematic of ratcheting phenomena.

The axial ratcheting strain (ε_r) is defined from Figure 2.8:

$$\varepsilon_r = \frac{(\varepsilon_{min} + \varepsilon_{max})}{2} \quad \text{..... (12)}$$

Where,

ε_{max} = maximum of axial strain in each cycle.

ε_{min} = minimum axial strain.

The axial Ratcheting strain rate is defined as the increment of ratcheting strain ε_r in each cycle and denoted as $\dot{\varepsilon}_r$. It is important in designing and life evaluation of the structural components endured in cyclic loading. Ratcheting strain is a secondary strain produced under asymmetrical cyclic stressing, and has a great dependence on loading conditions and loading history. Other factors, such as ambient temperature and non-proportionality of loading path, have significant effects on ratcheting. There are different types of structures that are subjected to cyclic loading where the stress state exceeds the elastic limit of the materials used. For design and analysis of these types of structures, accurate prediction of ratcheting response is critical as ratcheting can lead to catastrophic failure of the structures. Even for structures that are designed to be within the elastic limit, plastic zones may exist at discontinuities or at the tip of cracks. The fatigue cracks can initiate at these plastic zones. Therefore, better simulation model for cyclic plasticity response is important for the prediction of the high cycle fatigue life as well.

Most metals cyclically harden or soften up to a certain number of cycles and subsequently stabilize or cease to change the size of the yield surface. Ratcheting, though, keeps on occurring with cycles even after the material stabilizes. Hence, the kinematic hardening (translation of the yield surface in stress space) is attributed to be the primary reason for ratcheting. Ratcheting strain (ε_r) increase continuously with number of cycle (N) that indicates, plastic strain accumulated with time and material is finally failed due to high plastic strain. If ratcheting strain (ε_r) first increase with number of cycle (N) then comes to a constant value that indicates that in first portion of the curve plastic strain accumulated with time then stops, so material don't fail due to ratcheting [20].

2.9 Factors affecting ratcheting strain

2.9.1 Effect of mean stress and stress amplitude

In true stress controlled fatigue test S. K. Paul et. al [21] found ratcheting strain varies directly with the stress amplitude at constant mean stress, which is explained by the graph shown in Figure 2.9. In case of constant stress amplitude both ratcheting life and strain accumulation is increasing with tensile mean stress and strain accumulation paths are mirror of each other for tensile and compressive mean stress of equal magnitude. G. Chen et. al [22] concluded that ratcheting strain amplitude and ratcheting strain rate of 63Sn37Pb increased with increasing stress amplitude or mean stress correspondingly and also showed that ratcheting strain rate was very sensitive to the applied cyclic stress rate. Several other researchers have found that ratcheting strain depends on both mean stress and stress amplitude.[[23,24]

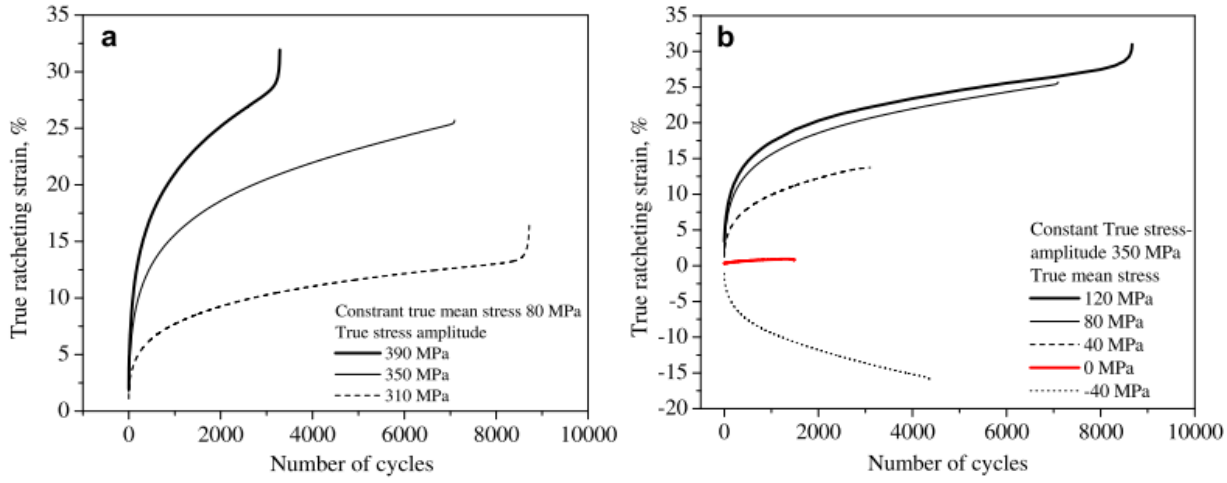

Fig. 2.9: True ratcheting Strain versus number of cycles: (a) constant σ_m : 80 MPa and σ_a : 310, 350 and 390 MPa (b) constant σ_a= 350 MPa and σ_m : -40, 0, 40, 80 and 120 MPa.

2.9.2 Effect of cyclic hardening/softening features

Ratcheting and failure behaviours of the materials depend greatly on the cyclic hardening/softening features of the materials. Kang et al. [4] studied the ratcheting behaviour of 25CDV4.11 steel and SS304 stainless steel. 25CDV4.11 steel features cyclic softening remarkably and SS304 stainless steel features cyclic hardening apparently which is shown in Figure 2.10 (a) and (b) respectively.

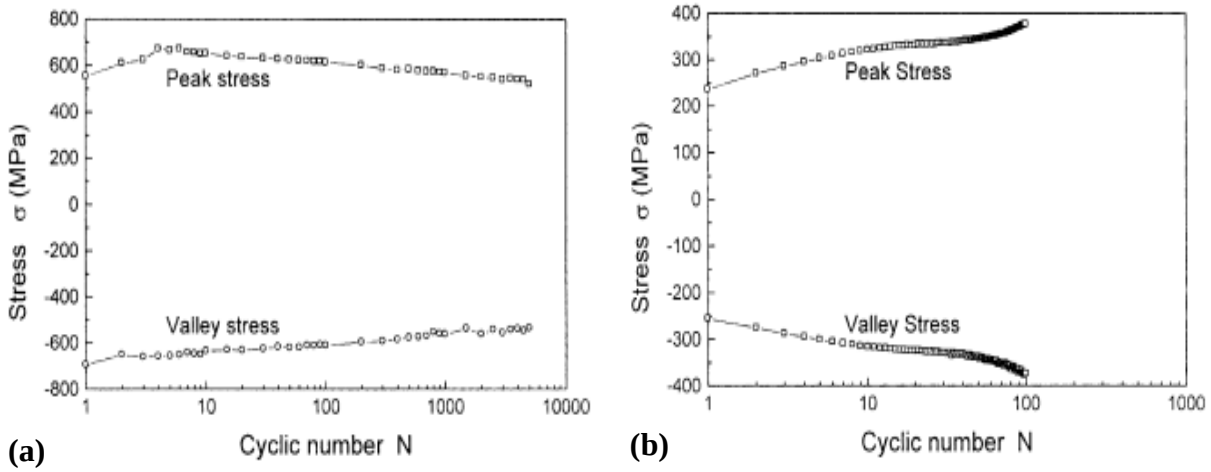

Fig. 2.10: Peak and valley stresses *vs* cyclic number N with various strain amplitudes for different: (a) 25CDV4.11, with strain amplitude 0.4% (b) SS304, with strain amplitude 0.8%.

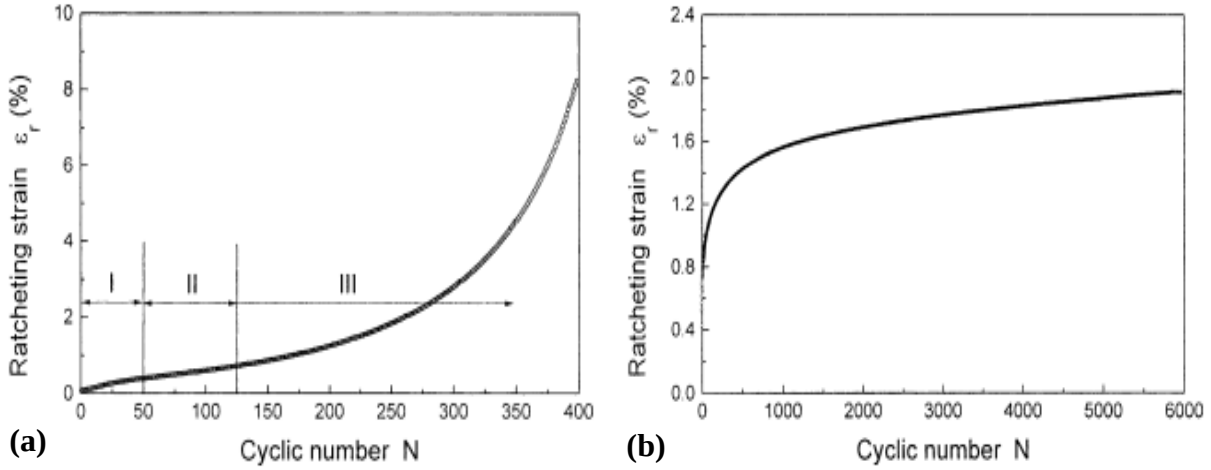

Fig. 2.11: Ratcheting strain *vs* cyclic number N of (a) 25CDV4.11 steel with load condition of 80 ± 600 MPa. (b) For SS304 with load condition of 65 ± 260 MPa.

When the material features cyclic softening behaviour, i.e., 25CDV4.11, ratcheting strain increases with cyclic number, no shakedown of ratcheting takes place and the material fails due to the increasing ratcheting strain regardless to the researched load conditions. When the material features cyclic hardening (i.e., SS304 stainless steel), the ratcheting strain rate decreases with the increase of cyclic number.

P.C. Lam et.al [25] studied initial hardening followed by progressive softening up to failure in case of aluminium-magnesium-silicon alloy. The stress response, deformation

characteristics and fracture behaviour of the alloy is interactively discussed in light of the competing influences of intrinsic microstructural contributions and deformation behaviour arising from a combination of mechanical and microstructural contributions. The softening occurred by a progressive decrease in stress for both the tension and compressive parts of a strain amplitude-controlled fatigue test is illustrated in Figure 2.11.

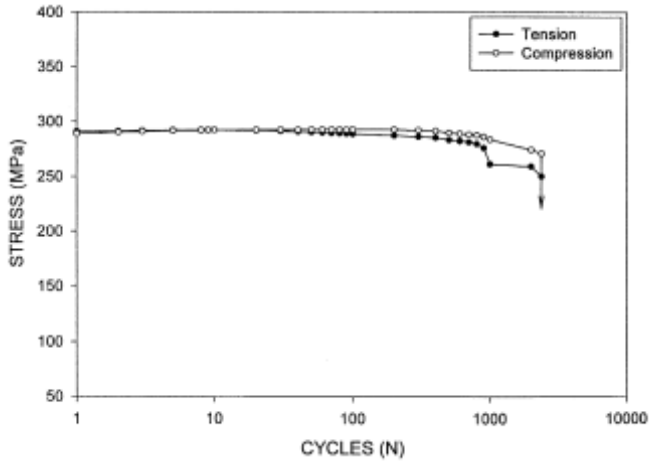

Fig. 2.11: Stress response curves showing the variation of tensile stress and compressive stress with cycles at fixed total strain amplitude of 0.60% [25].

2.9.3 Effect of stress rate

Ratcheting strain behaviour is giving the same nature as creep behaviour. Stages of ratcheting strain behaviour splits into three regions as the creep strain development under static load: the primary (transient), secondary (steady-state) and tertiary regions is studied by C. B. Lim et. al [26]. Ratcheting strain increases in a steady-state for much of the fatigue life at relatively low stress levels. Figure2.12. Represents the steady-state region diminishes at high stress levels.

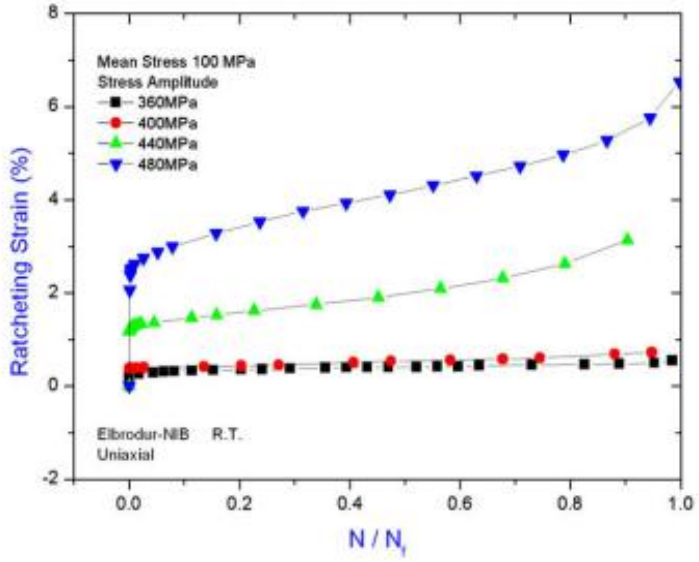

Fig. 2.12: Ratcheting strain versus life fraction under different σ_a with σ_m of 100 MPa [26].

These investigators have also found that ratcheting strain rate depends on the stress rate. Larger ratcheting strain was obtained at lower stress rates at all life fractions as shown in Figure 2.13. Ratcheting strain is decreasing with increasing mean stress.

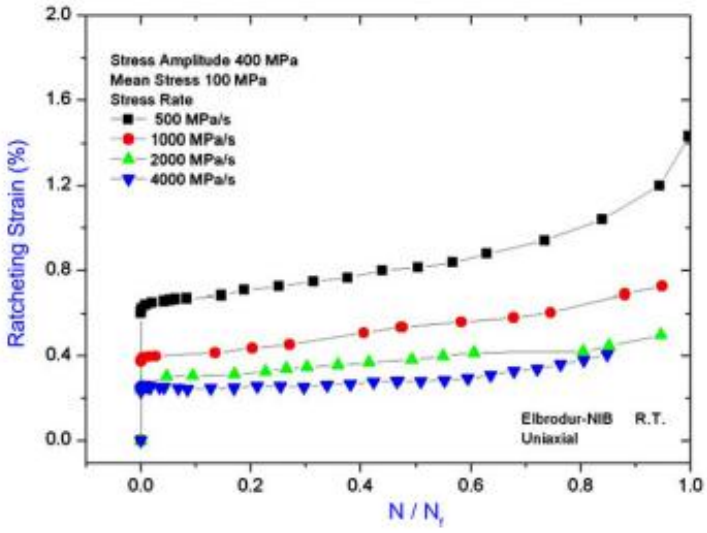

Fig. 2.13: Ratcheting strain versus cycle at different stress rates for σ_a : 400 MPa, and σ_m : 100 MPa [26].

2.9.4 Effect of extrusion ratio

X.P. Zhang et.al [27] presented the ratcheting behaviour of extruded AZ31B Mg alloy. The extrusion ratio did not influence the cyclic softening/hardening behaviour or the final ratcheting strain variation trend of the extruded AZ31B Mg alloy with the mean stress and the peak stress. However, the extrusion ratio influence the final ratcheting strain variation trend of the extruded AZ31B Mg alloy with the stress amplitude. Increasing the extrusion ratio also reduced the ratcheting strain and the effects of the load history on the ratcheting behaviour of the extruded AZ31B Mg alloy.

2.10 Materials on which Ratcheting behaviour have been studied

Ratcheting behaviour has been studied for cyclic hardening materials (such as SS304, 316FR and 316L stainless steel and cyclically stable such as U71Mn rail steel and ordinary carbon steels) [12,28]. Stress-controlled fatigue test has been conducted for ASTM A516 Gr 70 steel with tensile mean stress to study the effect of mean stress and ratcheting strain on fatigue life [29]. C. B. Lim et. al studied the ratcheting and fatigue behaviour for copper alloy at room temperature with and without σ_m [26]. Ratcheting is also studied for the materials, which are prepared by using powder metallurgy. The cyclic deformation behaviour of two dispersion-strengthened aluminum alloys produced by mechanical alloying is examined. The results of plastic strain-controlled low cycle fatigue tests are compared with those obtained for a conventional A1-Mg alloy (AA5083-H321) and a conventional precipitation-strengthened alloy (AA7075-T6) [30]. The effect of annealing treatment on the ratcheting behaviour and variation in microstructure and monotonic tensile properties is assessed for extruded AZ31B magnesium alloy [27]. However the ratcheting behaviour of materials is a complex phenomenon. It depends on a number of factors including mean stress, stress amplitude, frequency, loading history and micro-structural characteristics. Uniaxial ratcheting characteristics of 63Sn/37Pb at room temperature studied experimentally and particular attention is given to ratcheting behaviour under different loading rates [22]. Kang et. al [4], found that cyclic hardening materials fails due to combined effect of increasing ratcheting strain and low cycle fatigue, while cyclic softening materials fails under large ratcheting strain. The effect of σ_a, σ_m, loading history and stress ratio on the ratcheting behaviour of high-nitrogen steel was also analyzed [31,32]. Ratcheting deformation is microscopically related to the mobility of dislocation during the cyclic loading; it is supposed that the metals

with different crystal structures or values of fault energy shall present more or less different ratcheting behaviours [33]. Ratcheting behaviours of metals with different crystal structures or values of fault energy was observed by the uniaxial stress-controlled cyclic tension-compression tests with non-zero mean tensile stress [34]. Microstructural changes during cyclic loading have been reported by C. E. The hysteresis loops for materials having a wavy slip character (high stacking fault energy) are virtually symmetrical with respect to both the stress and strain axes. On the other hand, for materials having a planar slip character (low stacking fault energy) the loops are always displaced with respect to the strain axis in the direction of the first applied stress. [33,35]. The fatigue failure process exploits the weakest links (discontinuities) within the test material, which act as nucleation sites for crack origins [36].

2.11 Theoretical study on ratcheting

In recent years, a series of theoretical studies on ratcheting have been conducted [37-42,]. It can be mentioned that kinemetic hardening is the main mechanism of ratcheting behaviour. It is defined as the hardening of solid due to high stress applied on it. It will take place when the yield surfaces preserve their shape and size but translate in the stress space as a rigid body [17,43-44]. A number of constitutive model have been proposed to describe the elastoplastic behaviour under cyclic loading conditions [45]. Armstrong and Frederic model is used in the theory of inelastic deformations of metals. This model simulates the multiaxial Bauschinger effect, when compared to the previously existing models, intuitively one would be expected, for example, the uniaxial cyclic loading test [40]. When compared to experimental results, Armstrong Frederick predictions were more accurate than previous models for cyclic axial loading and torsion-tension of a thin tube tests on annealed copper.

CHAPTER - 3

EXPERIMENATAL

3.0 Introduction

The experiments that have been carried out in the present investigation are presented in this chapter. It includes heat treatment, material characterization, fatigue test, post-fatigue tensile test and fractographic observation.

3.1 Material selection

Commercial pure aluminium was chosen for this investigation. Initially the material was in the form of rods, the diameter of each rod was 18 mm.

3.2 Chemical composition analysis

Chemical compositions of the selected rods were studied by using an optical emission spectrometer (Model MA 3460, Thermo Electron, Switzerland). Two measurements were carried out using optical emission spectroscopy (OES) for both qualitative and quantitative estimation of impurity elements present in the commercial pure aluminium. The chemical composition of pure Al, obtained by OES is shown in Table 4.1.

3.3 Heat treatment

The purpose of heat treatment is to soften the material, to change the grain size, to modify the structure of the material and to relieve the stress set up in the material after hot and cold working. In this investigation, we have used annealing and normalising. One set of rods were annealed and other set normalised.

3.3.1 Annealing

- Heating the samples to a predetermined temperature of 200°C in a furnace.
- Soaking, i.e., holding the samples at this temperature for 30 minutes to obtain homogeneous structure.
- Samples were cooled in a furnace by switching it off.
- Samples were taken out from the furnace after reaching the furnace temperature to room temperature.

3.3.2 Normalising

- In this process heating temperature and soaking time is same as annealing but cooling rate is different.
- Samples were heated to a predetermined temperature of 200^0C.
- Soaking at 200°C temperature for 30 minutes to obtain the homogeneous structure.
- Then samples were taken out from furnace by switching it off.
- Samples were cooled in air.

3.4 Metallography

Samples of approximately 10 mm height were cut from the annealed and normalised rods for microstructural studies. Samples were rough ground on a belt grinder by slowly moving it up and back across the surface of a flat smooth file, with the samples kept cool by frequent dropping in water during the grinding operation. In all grinding and polishing operations the specimen was moved perpendicular to the existing scratches. It was continued until the surface is flat and free of nicks, burr etc. After rough grinding the samples were polished by series of emery papers containing successively finer abrasive. The polishing was done by 1/0 grade then 2/0, 3/0 and last 4/0. The final approximation to a flat scratch-free surface was obtained by the use of a wet rotating wheel covered with a special cloth that was charged with carefully sized abrasive particles.

After fine polishing samples were thoroughly cleaned with soap solution, and subsequently dried using drier. Samples were etched with Keller's Reagent [2ml HF (1%), 3ml HCl (1.5%), 5ml HNO_3 (2.5%), and 190 ml H_2O (95%)].

3.4.1 Optical Microscopy

The samples were examined by optical microscope (Model: Olympus BX61), and images were recorded at different magnifications. Optical microscope is shown in Figure 3.1 (a).

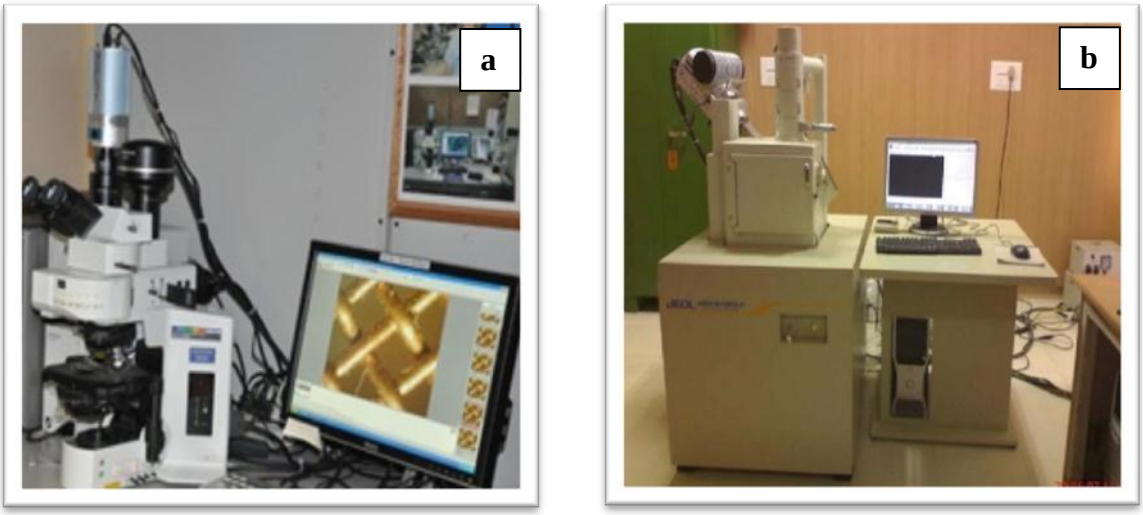

Fig. 3.1: (a) Optical Microscope (b) Scanning Electron Microscope

3.4.2 Scanning electron microscopy

Microstructures of the annealed and normalised aluminium were examined using a scanning electron microscope (SEM) (Model: JEOL-JSM 6480LV) equipped with an energy dispersive X-ray (EDX) for compositional analysis. The SEM was operated at an accelerated voltage of 20 kV. Figure 3.1 (b) shows the scanning electron microscope. Both secondary (SE) and back-scattered electron (BSE) imaging modes were used to study the microstructures. EDX technique was used for chemical characterization of sample.

3.4.3 Grain size measurements

The average grain size of the aluminium was determined with the linear intercept method according to ASTM standard E-112 [46]. In this method, a linear test grid was superimposed on the microstructure and the number of aluminium grains intercepted by the test line was counted. Such measurements were repeated on 50 randomly chosen fields at a magnification of 500X. The average grain size was then calculated using the relation:

$$d = L_T/N_L \quad \text{..... (13)}$$

Where,

N_L = number of grains intercepted by a unit true test line length.

L_T = the true length of a test line is defined as the length of the test line at unit magnification.

3.4.4 Hardness Determination

The specimens for hardness measurements were first ground flat and parallel to each other using a belt grinder to ensure accuracy of measurements. The samples were then mechanically polished using the procedure mentioned in section 3.4. Vickers hardness tests were carried out with the help of a Vickers Hardness Tester (Model: Leco LV 700), which is shown in Figure 3.2.

Fig. 3.2: Leco LV 700 Vickers hardness tester.

The hardness was measured at a normal load of 3 kgf. At least 3 readings were considered for each sample to calculate the average hardness. The Vickers hardness was calculated using the expression:

$$H_V = \frac{1.854P}{d_{avg}^2} \quad \text{..... (14)}$$

Where,

P = indentation load.

$d_{avg} = \frac{(d_1+d_2)}{2}$, in which d_1 and d_2 are the lengths of two indentation diagonals.

3.5 Mechanical Testing

3.5.1 Tensile properties determination

Round bar specimens, having gauge length 20 mm and diameter 10 mm were fabricated from annealed and normalised rod of 200 mm in length and initial diameter was 18 mm according to ASTM standard E-606 [47]. Typical configuration of a tensile specimen is shown in Figure 3.3.

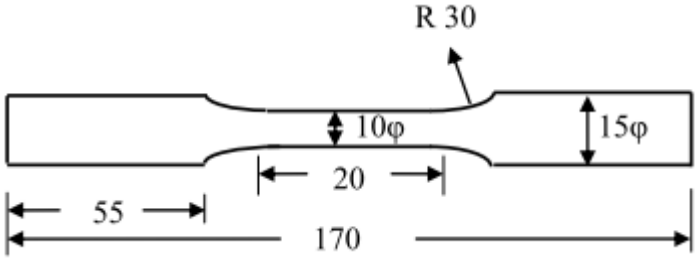

Fig. 3.3: Specimen design for fatigue testing.

Specimens were polished using lathe machine up to fine polishing. The specimens were tested till fracture using an INSTRON 8800 testing machine at room temperature. These tests were carried out at a crosshead speed of 1 mm/min. For each test, the load displacement signals were automatically recorded, and the digital values of load and displacement were stored in a computer data file for subsequent processing.

Fig. 3.4: Servo hydraulic INSTRON 8800 machine.

3.5.2 Fatigue Study

Stress controlled fatigue tests were carried out at room temperature up to 150 cycles using servo-hydraulic testing machine (Model: INSTRON 8800). All controls and data acquisition were done in stress-control mode at a constant stress rate of 50MPa/s. The variables that have been considered for these tests are mean stress (σ_m) and stress amplitude (σ_a). Test matrix for the annealed and normalised conditions is given in Table 3.1 and Table 3.2. Based on the employed test controls, the test can be classified into two categories (i) constant σ_m with varying σ_a (ii) constant σ_a with varying σ_m. Fatigue test of the specimens were done up to 150 cycles. During each test the load-extension as well as the actuator displacement data was continuously recorded by using attached software to the computer. It was aimed to acquire at least 200 data points per cycle during fatigue tests.

Test matrix for fatigue test

Table 3.1: Test matrix for fatigue test in annealed condition

Serial No	Mean stress (σ_m) MPa	Stress amplitude(σ_a) MPa
1	40	175, 185
2	45	175, 185
3	50	175, 185

Table 3.2: Test matrix for fatigue test in normalised condition

Serial No	Mean stress (σ_m) MPa	Stress amplitude(σ_a) MPa
1	30	170, 180
2	35	170, 180
3	40	170, 180

3.5.3 Post Fatigue Tensile Tests

After completion of 150 cycles during cyclic loading, the same specimens were subjected to tensile test at a crosshead speed of 1mm/min. This crosshead speed corresponds to a nominal strain rate of 0.83×10^{-5} s^{-1}. During these tests also, the load displacement signals were automatically recorded, and the digital values of load and displacement were stored in a computer data file for subsequent processing.

3.6 Fractography

Transverse sections were cut from the gauge portion after post fatigue tensile test by using hacksaw. Fracture surface of the samples were taken by scanning electron microscopy (SEM) at different magnifications 1000X, 2000X and 5000X. For determining the phases present at the inclusion sites EDS analysis were done.

3.7 Post-fatigue hardness

After cutting of fracture surface for fractography, to determine the hardness transverse section were cut from the gauge portion of 10 mm height. Specimens were polished up to fine polishing for determining the Vickers hardness.

In summary, in this chapter, all the experiments which are carried out during this investigation, is discussed. Photographs of testing systems which were employed during the course of this investigation are also illustrated in this chapter.

CHAPTER – 4

RESULTS & DISCUSSION

4.0 Introduction

Various experimental results that have been developed during this investigation are reported here along with their pertinent discussion. It consist results and discussion based on chemical composition, microstructural analyses and mechanical property tests.

4.1 Chemical composition

The chemical composition of pure Al, obtained by OES is shown in Table 4.1. The OES results indicate that the purity of the investigated Al is very close to about 99%. The major impurities those are present in the sample are Mg, Fe, Ti and V, although Mn, V and Zr are in traces.

Table 4.1: The chemical composition (in wt %) of selected aluminium

Element	Si	Mg	Fe	Ti	Mn	V	Zr	Al
Wt%	0.51	0.46	0.17	0.02	0.007	0.005	0.004	98.824

4.2 Microstructural Analysis

The microstructure of the investigated aluminium reveals equiaxed grains. The grain boundaries are very clearly observed. Typical optical micrograph of annealed aluminium is illustrated in Figure 4.1 (a). SEM micrographs of aluminium were taken at different various magnifications. A typical SEM micrograph is illustrated in Figure 4.1 (b). Grain size of aluminium is estimated by using linear intercept method according to ASTM standard E112 [46]. It was found that average grain size is 50.63µm.

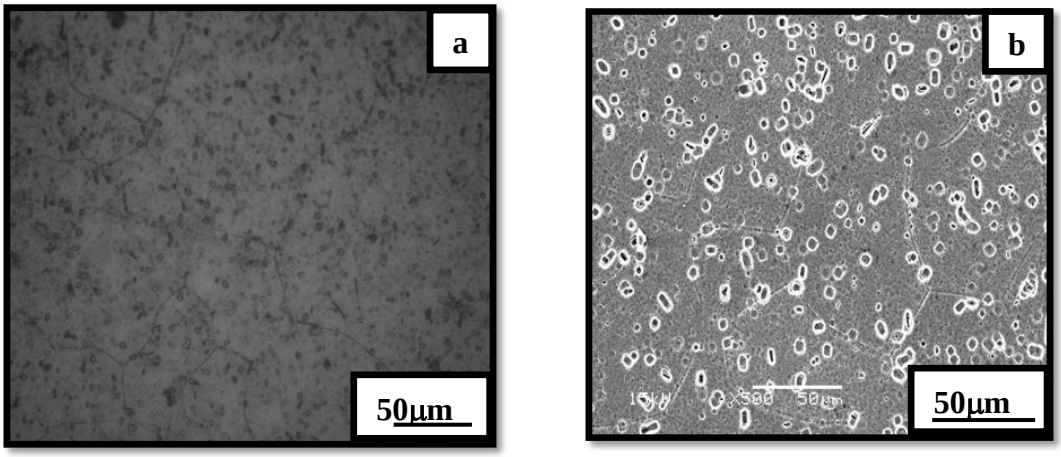

Fig. 4.1: (a) optical micrograph of aluminium (b) SEM micrograph of aluminium.

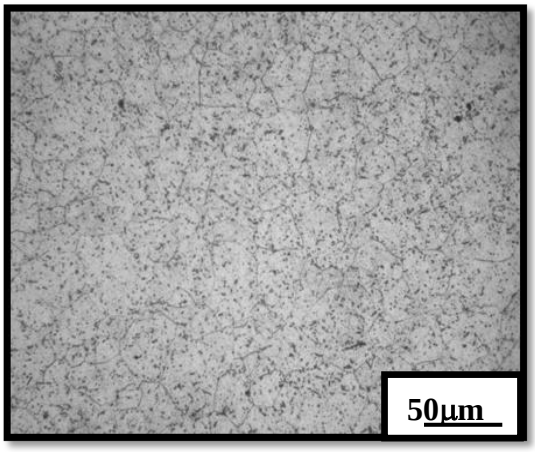

Fig. 4.2: Optical micrograph of normalised aluminium.

For further determination of the impurity elements which are present in aluminium we have done EDS experiments. EDS spectra of investigated sample is shown in Figure 4.3. From this figure we can observe that there are two peaks present at lower potential, lower intensity peak represent manganese and higher intensity peak represents aluminium. Then it is clear that along with high amount of aluminium some amount of manganese is present. These results are not perfectly in line with our OES results, although it can be concluded that very little amount of other impurities are present in the investigated material.

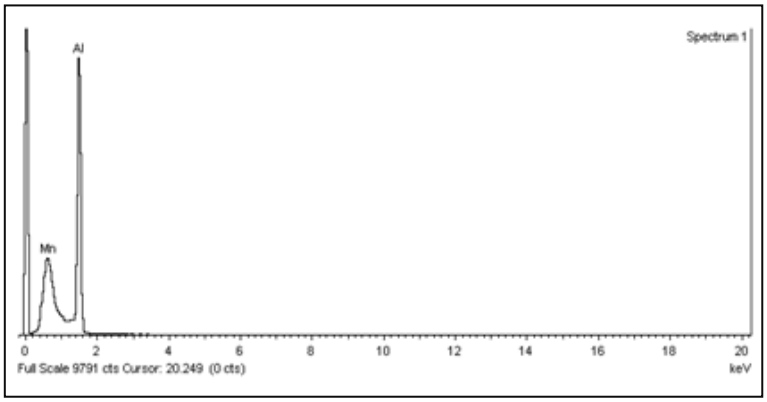

Fig.4.3: EDS Spectra of aluminium.

4.3 Hardness

Hardness of investigated aluminium samples have been measured in different heat treatment conditions by Vickers hardness tester. At least three readings have been taken at different

positions for a comparative assessment; both for annealed and normalised samples. The results are tabulated in Table 4.2.The dwelling time is 15 s, with applied load of 3 kgs.

Table 4.2: Vickers hardness in annealed and normalised condition

Heat treatment condition	D_1 (μm)	D_2(μm)	VHN	Average VHN
Normalised	252.2 249.5 247.4	249.5 247.8 252	88.4 90.16 89.2	89.2
Annealed	253.9 256.5 258.4	256.9 257.4 258.4	85.3 86.3 83.3	86.26

4.4 Tensile Properties

From the load and elongation values, obtained from the servo-hydraulic testing machine, corresponding stress and strain is calculated and plotted to get stress vs. strain curves in annealed and normalised conditions. Figure 4.4 and Figure 4.5 shows the engineering stress-strain curve in annealed and normalised condition. Results of tensile tests are tabulated in Table 4.3 for both annealed and normalised conditions. For both the cases it is observed that there is no sharp yield point, so yield strength is determined by the stress corresponding to the intersection of the stress-strain curve and an offset line parallel to the elastic portion of the curve at a strain of 0.2%.

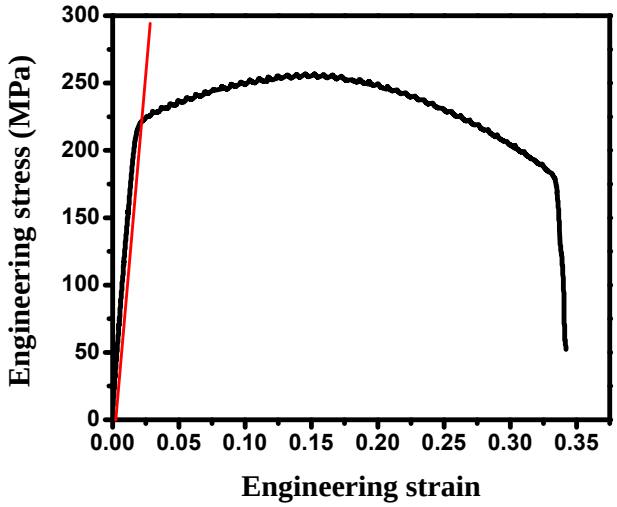

Fig. 4.4: Engineering stress-strain curve in annealed condition.

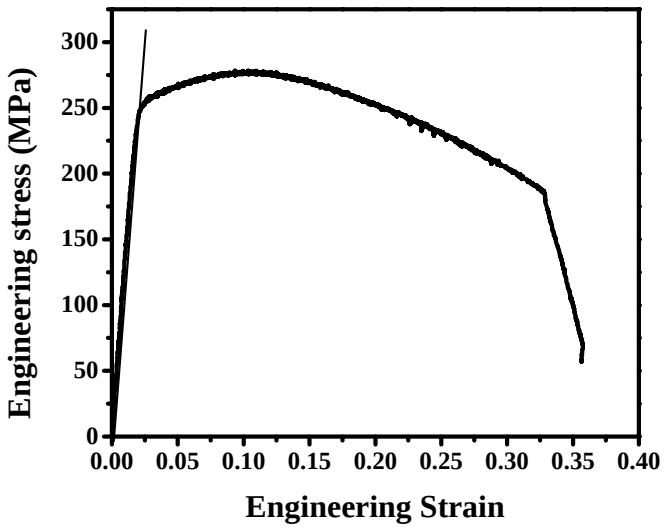

Fig. 4.5: Engineering stress-strain curve in normalised condition.

Table 4.3: Tensile properties of investigated aluminium

Heat treatment condition	Yield strength	Tensile strength	Uniform elongation % (e_u)	Total elongation % (e_t)
Annealed	221 MPa	256 MPa	14.55	34.20
Normalised	246MPa	278MPa	10.75	32.55

Histogram presented in Figure 4.6 gives the comparative analysis of tensile properties in different heat treatment conditions. From this graph it is clear that in case of normalised condition strength of material is more in comparison to annealed. This can be explained by the optical microstructure which has been shown in Figure 4.2. In case of normalised condition grain size is fine in comparison to the normalised condition. With the help of Hall Petch equation [1], fine grain size is responsible for increase in strength of normalised condition.

$$\sigma_y = \sigma_0 + kd^{\frac{-1}{2}} \quad \text{..... (15)}$$

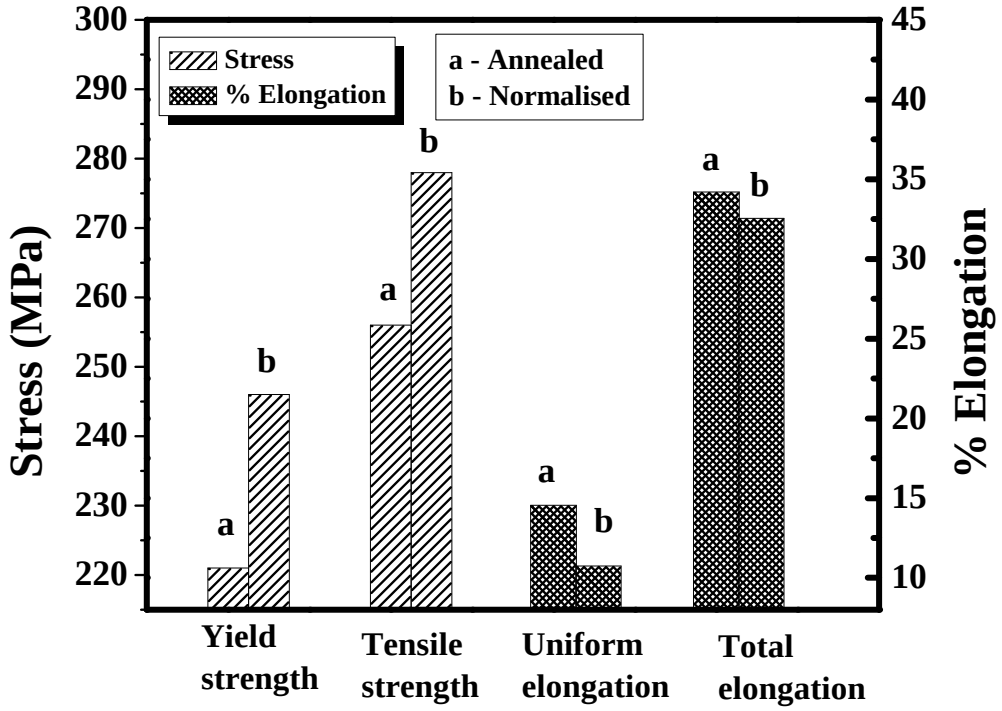

Fig. 4.6: Comparison of mechanical properties of aluminium in annealed and normalised condition.

4.5 Analyses of Fatigue Tests

The results of cyclic tests conducted up to 150 cycles under different combinations of mean stress (σ_m) and stress amplitude (σ_a) in annealed and normalised heat treatment conditions are presented and discussed in this section. Y. Liu et al. [48] studied the ratcheting behaviour of 6061-T6 aluminium alloy till fracture and observed that saturation in ratcheting strain is taking place after 60 cycles. In steel saturation is taking place after 100 cycles [23].To study the post fatigue tensile properties we have selected to do fatigue tests up to 150 cycles; it was established from the current set of tests that 150 cycles are well above the saturation level.

Typical hysteresis loops those were generated during fatigue tests at σ_m= 40 MPa, σ_a= 180 MPa and σ_m = 45MPa, σ_a = 200 MPa are presented in Figure 4.7 and Figure 4.8 respectively. Figure 4.7(a) shows the hysteresis loop of first and second cycles for σ_m = 40 MPa, σ_a = 180, where point P and Q represents the minimum and maximum strain for this cycle. Strain accumulation is calculated by taking the average of minimum and maximum strain in particular cycle. Figure 4.7 (b) represents the hysteresis loops up to 150 cycles.

From this graphs it is clear that hysteresis loops shift towards more strain direction during ratcheting deformation, which in turn induces plastic strain to the material. The hysteresis loop for first cycle and up to 150 cycles is given in Fig 4.8(a) and Fig 4.8(b) respectively for the stress condition of σ_m= 45MPa, σ_a = 200 MPa. The strain accumulation is more for the second case as is discussed in detail in the upcoming sections.

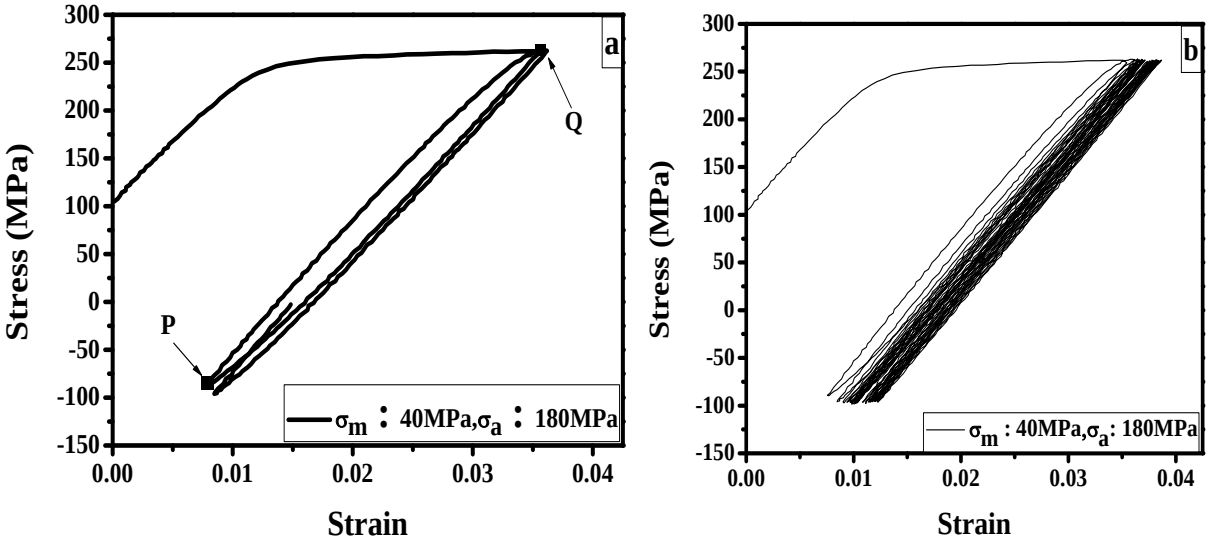

Fig.4.7: (a) Hysteresis loop for first cycle (b) hysteresis loops up to 150 cycles at σ_m : 40 MPa, σ_a : 180 MPa.

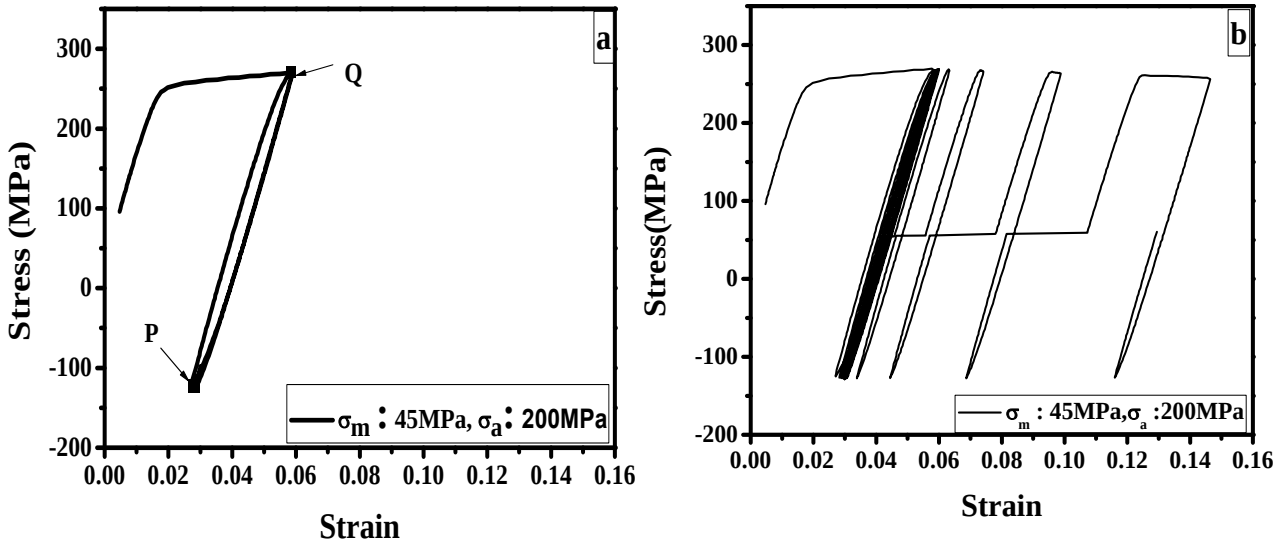

Fig.4.8: (a) Hysteresis loop for first cycle (b) hysteresis loops up to 150 cycles at σ_m : 45MPa, σ_a : 200 MPa.

4.5.1 Strain accumulation: Effect of stress amplitude at constant mean stress

The variation of ratcheting strain (ε_r) with number of cycles (N) for varying σ_a = 175, 185 MPa at constant σ_m (40, 45, 50MPa) is examined. A typical plot of ε_r *vs* N in annealed condition is shown in Figure 4.9 at constant σ_m = 45MPa and varying σ_a= 175, 185 MPa. The results indicate that ratcheting strain increases monotonically with increasing number of cycles for any σ_a-σ_m combination. There are two stages is achieved in graph initially very high rate of increase of strain accumulation and after that saturation is achieved. The cyclic loading stopped at 150 cycles for doing post-fatigue tensile test. A few specimens have broken before reaching 150 cycles. For these samples post-fatigue tests could not be done.

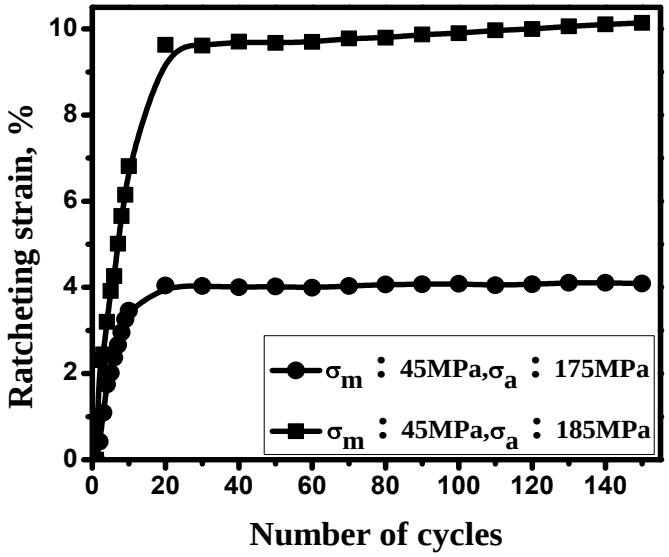

Fig. 4.9: Variation of ε_r with number of cycles in annealed condition for varying σ_a (175, 185 MPa) at constant σ_m : 45MPa.

Histogram presented in Figure 4.10 clearly shows the increase of ε_r with number of cycles at constant σ_m = 45 MPa. For σ_m = 45 MPa, σ_a = 175 MPa strain accumulation is 4.05 % and it increased to 10.14 % on increasing the σ_a up to 185 MPa.

On increasing the σ_a, maximum stress (σ_{max}) is increasing while minimum stress (σ_{min}) is decreasing. Due to this fact, the area of hysteresis loop increases. Shifting of hysteresis loop is observed in more strain direction with increasing number of cycles. In existing database we observed that strain accumulation is increased due to dislocation density [23]. Due to shifting of hysteresis loop dislocation density is increasing. Increased area of hysteresis loop causes the increased strain accumulation with σ_a.

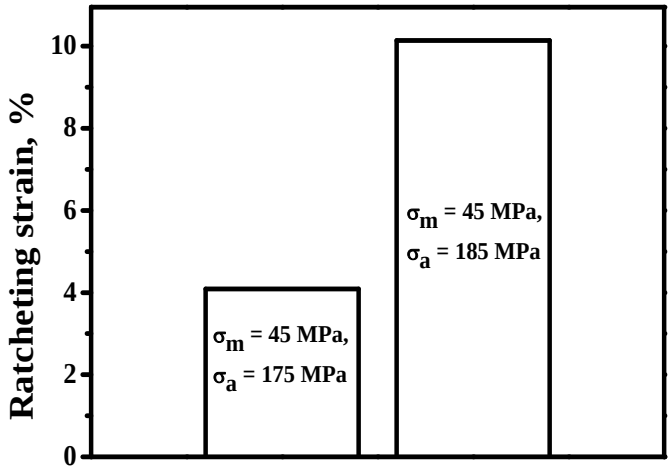

Fig. 4.10: Histogram showing the variation of $\varepsilon_r$for varying σ_a (175, 185 MPa) at constant σ_m : 45MPa.

To study the strain accumulation behaviour in case of normalised condition similar tests have been performed under different combination of σ_m (30, 35, 40 MPa) and σ_a (170, 180 MPa). Figure 4.11 and Figure 4.12 illustrate the effect of σ_a (170, 180 MPa) at constant σ_m level of 30 and 40 MPa on ε_r respectively. Figure 4.11 shows that at lower stress amplitude σ_a = 170MPa strain accumulation is rapid up to 10 cycles. Saturation in strain accumulation is achieved after 10 cycles. But in case of σ_a = 180 MPa saturation in strain accumulation is not achieved, strain accumulation is continuously increasing with increasing number of cycles. 0.13 % strain accumulation is obtained for σ_m = 30 MPa, σ_a = 170 MPa, on increasing the σ_a to 180 MPa strain accumulation has been reached up to 0.38% in 150 cycles.

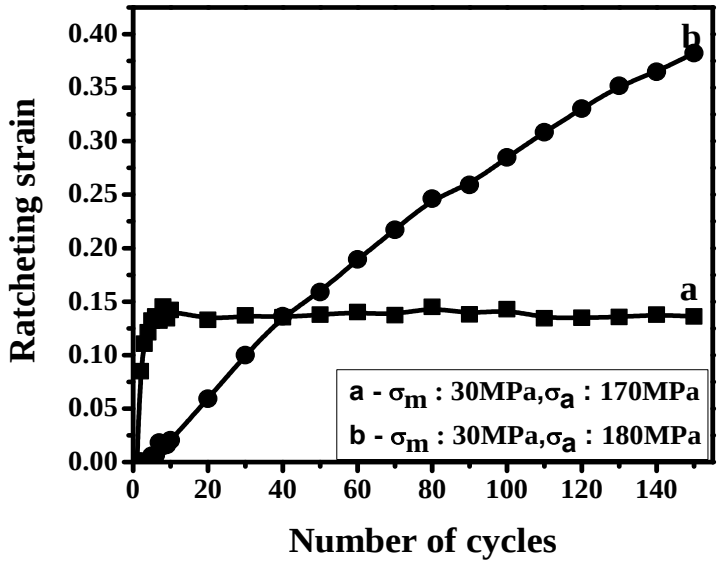

Fig. 4.11: Variation of ε_r with number of cycles in normalised condition for varying σ_a (170, 180 MPa) at constant σ_m : 30MPa.

Figure 4.12 represents the effect of σ_a (170, 180 MPa) at constant σ_m= 40MPa. 0.50 % and 0.82 % strain accumulation is achieved for σ_a = 170 MPa and 180 MPa at constant σ_m = 40 MPa respectively. In this case ε_r increasing with number of cycles for both σ_a 170 MPa and 180 MPa saturation in strain accumulation is achieved after few cycles. In case of lower σ_m strain accumulation behaviour is not exactly same as annealed behaviour but at σ_m= 40 MPa strain accumulation behaviour is same for both annealed and normalised condition.

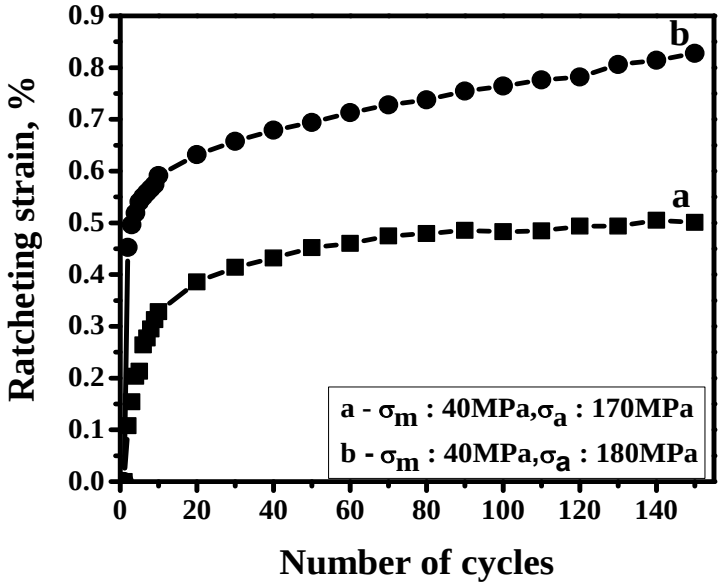

Fig. 4.12: Variation of ε_r with number of cycles in normalised condition for varying σ_a (170, 180 MPa) at constant σ_m : 40 MPa.

4.5.2 Strain accumulation: Effect of mean stress at constant stress amplitude

As the mean stress is varied at constant levels of σ_a, the behaviour of strain accumulation is found similar, as discussed in the previous section. Figure 4.13 and Figure 4.14 illustrate the effect of increasing σ_m of 40, 45, 50 MPa with constant σ_a levels of 175, 185 MPa on ε_r in annealed condition respectively. From these graphs it is clear that strain accumulation is increasing with increasing σ_m. For σ_m= 40 MPa, σ_a= 175 MPa strain accumulation is 1.25 % on increasing the σ_m to 45 MPa strain accumulation has been reached up to 4.09 %.For the case of σ_m = 50 MPa, the strain accumulation is very rapid and the specimen breaks after first few cycles. As a consequence, post–fatigue tensile test could not be done for this case. Increase of ε_r with increasing σ_m level of 40, 45, 50 MPa at constant σ_a = 175 MPa is explained by histogram shown in Figure 4.15.

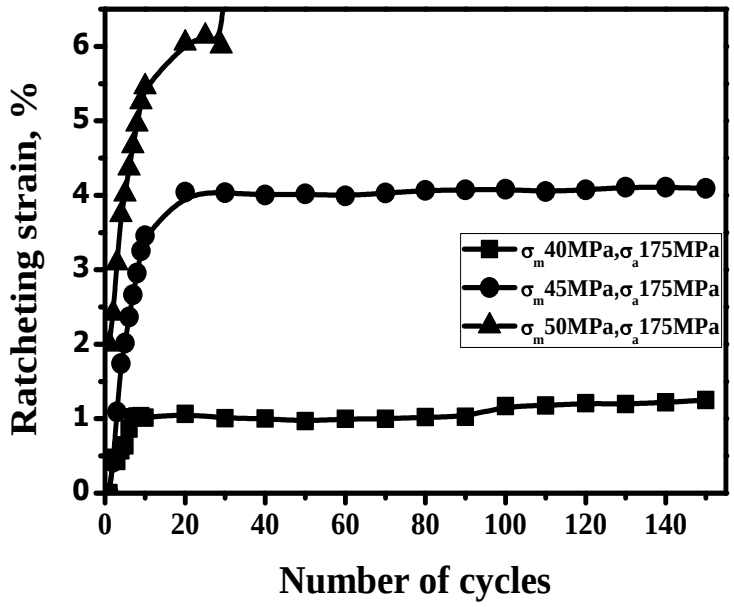

Fig.4.13: Variation of ε_r with number of cycles in annealed condition for varying σ_m (40, 45, 50 MPa) at constant σ_a : 175MPa.

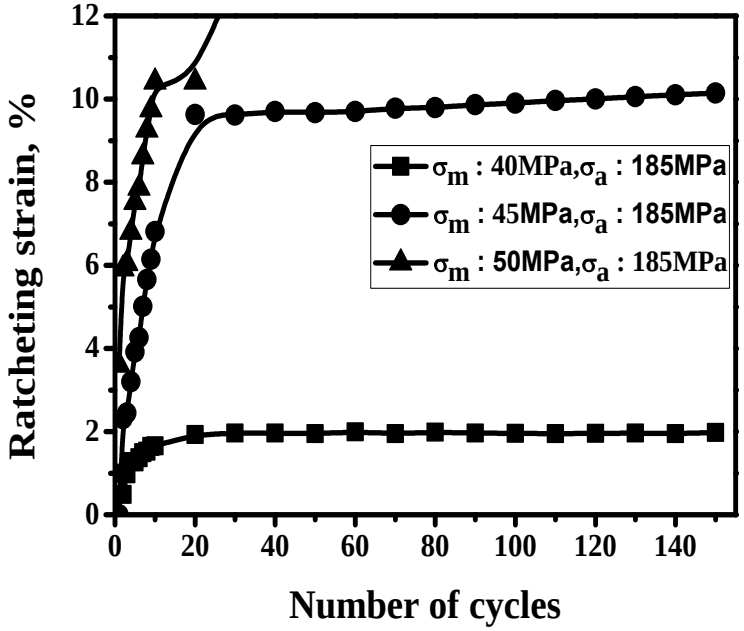

Fig.4.14: Variation of ε_r with number of cycles in annealed condition for varying σ_m (40, 45, 50 MPa) at constant σ_a : 185 MPa.

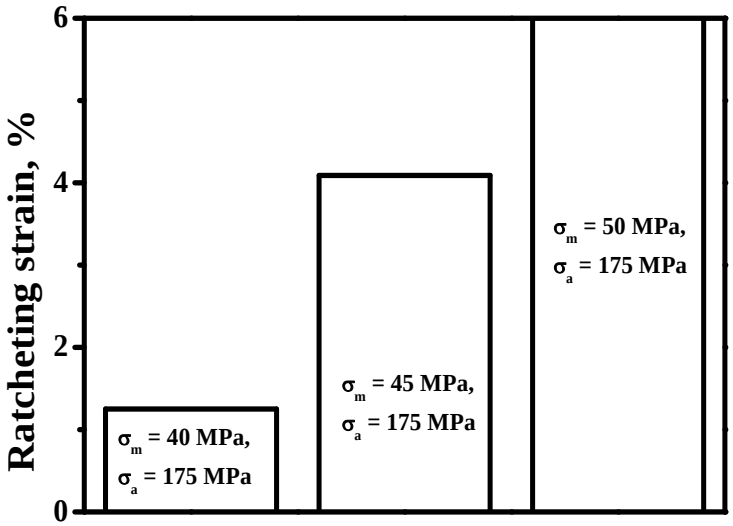

Fig. 4.15: Histogram showing the variation of ε_r for varying σ_m (40, 45, 50 MPa) at constant σ_a : 175 MPa.

To delineate the increase in strain accumulation with increasing mean stress, a schematic diagram of shifting of hysteresis loops is presented in Figure 4.16 (at constant σ_a). In case 1 σ_m is lower in comparison to case 2. Both maximum and minimum stresses are increasing with increasing σ_m, which results in the shifting of hysteresis loops in upward direction.

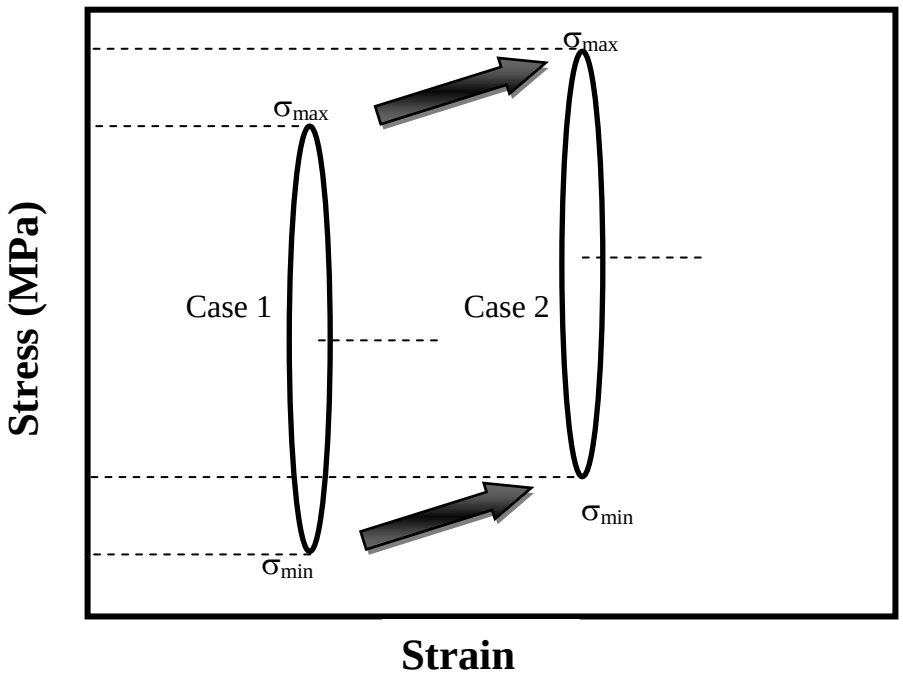

Fig.4.16: Shifting of hysteresis loop for varying σ_m at constant σ_a.

To compare it with the actual case, let us consider typical cases. In case of σ_m = 40 MPa with σ_a = 175 MPa, we get maximum and minimum stresses as 215 MPa and -135 MPa respectively. But there are increase in maximum and minimum stress values as 220 MPa and -130 MPa respectively, as when σ_m = 45 MPa and σ_a = 175 MPa. This fact causes increasing amount of dislocation generation when mean stress is increased to higher level, as is mentioned by K. K. Ray et. al [23]. The increase in strain accumulation with increasing mean stress can be described as a consequence of increasing dislocation density, at higher mean stress levels. Although some transmission election microscopy may reveal this fact more accurately, this could not be done during the current investigation.

Figure 4.17 and Figure 4.18 illustrate the effect of σ_m at constant σ_a levels of 170, 180 MPa on ε_r in annealed condition respectively. Figure 4.17 illustrates the effect of σ_m (30, 35, 40 MPa) at constant σ_a = 170 MPa. For σ_m = 30 MPa and σ_a = 170 MPa strain accumulation is 0.14 %, when σ_m is increased to 35 MPa, strain accumulation is decreased to 0.00083 %. However in case of σ_m = 40 MPa strain accumulation is 0.50 %. Figure 4.18 illustrates the effect of σ_m at constant σ_a = 180 MPa. From these graphs it is clear that strain accumulation is very less for σ_m = 35 MPa at both σ_a level 170 and 180 MPa.

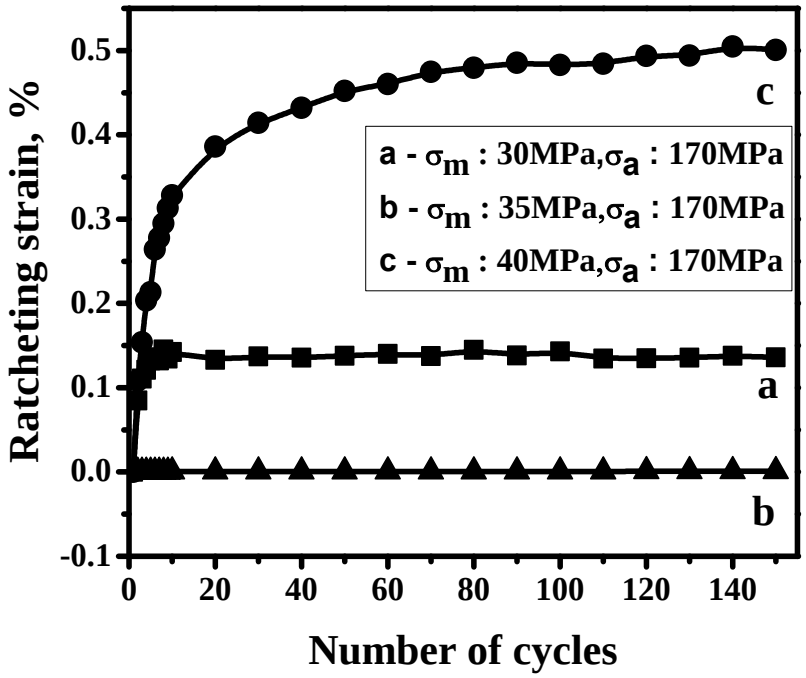

Fig.4.17: Variation of ε_r with number of cycles in normalised condition for varying σ_m (30, 35, 40 MPa) at constant σ_a : 170 MPa.

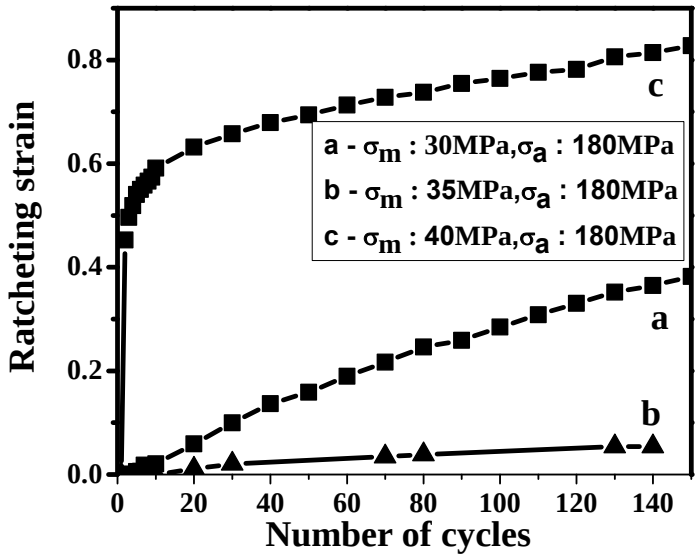

Fig.4.18: Variation of ε_r with number of cycles in normalised condition for varying σ_m (30, 35, 40 MPa) at constant σ_a : 180 MPa.

4.5.3 Saturation in strain accumulation

The graph between rate of strain accumulation ($\dot{\varepsilon}_r$) *vs* N is plotted by differentiating the graph between ε_r *vs* N. Figure 4.19 shows the graph between rate of strain accumulation and number of cycles at constant σ_m = 45 MPa in annealed condition. The results indicate that $\dot{\varepsilon}_r$ is rapidly decreasing up to 10 cycles, then it is growing towards saturation slowly decreasing up to 40 cycles after that saturation in strain accumulation is achieved.

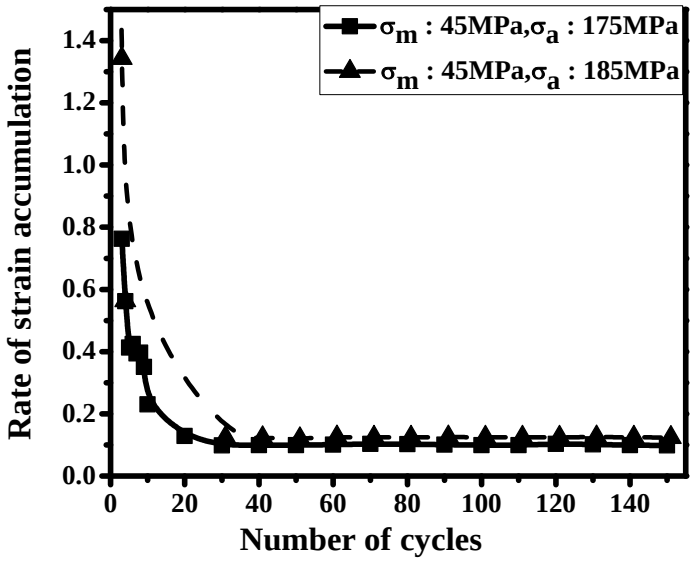

Fig. 4.19: Variation in Rate of strain accumulation with number of cycles in annealed condition for varying σ_a (175, 185 MPa) at constant σ_m : 45 MPa.

In the same way saturation in strain accumulation is determined for normalised condition. Figure 4.20 illustrate the saturation in strain accumulation for σ_a = 170 MPa. Saturation in strain in accumulation is achieved after 30cycles. Saturation takes place due to attainment of stable dislocation configuration after initial few cycles.

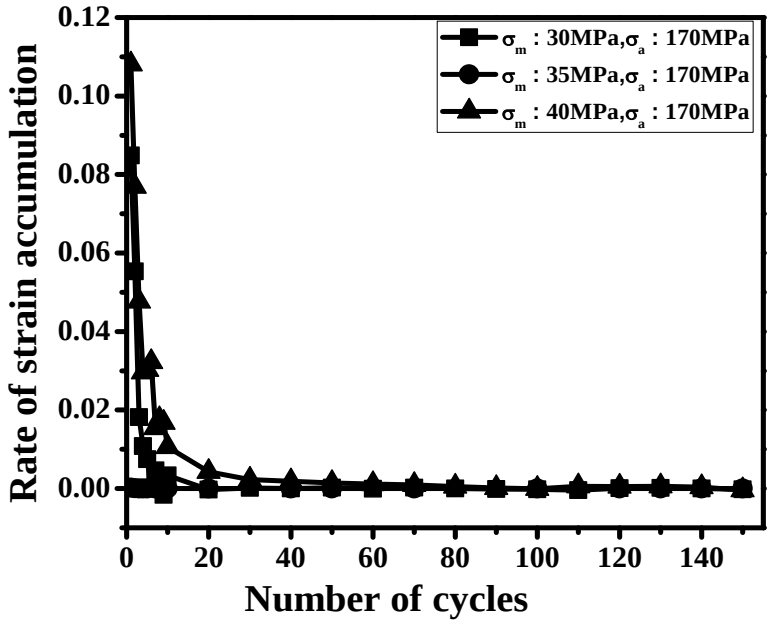

Fig. 4.20: Variation in Rate of strain accumulation with number of cycles in normalised condition for varying σ_m (30, 35, 40 MPa) at constant σ_a : 170 MPa.

In normalised condition saturation in strain accumulation is achieved in earlier cycles in comparison to the annealed condition. This occurs due to the fact that the dislocations find a barrier more quickly in normalised samples as the grain size is lower in case of normalised samples.

4.5.4 Post-fatigue tensile properties: Effect of stress amplitude at constant mean stress

The variation in post-fatigue tensile properties for varying σ_a (175, 185 MPa) at constant σ_m level of 40 and 45 MPa have been examined. Figure 4.21 illustrates the effect of σ_a at constant σ_m = 40 MPa on post-fatigue tensile properties. In this graph, curve (a) represents the tensile stress-strain curve for a sample which was not subjected to any ratcheting test. Curve b and c are obtained by doing fatigue test up to 150 cycles which was followed by a tensile test to study the variation in post- fatigue tensile properties. From this graph it is clear that

yield strength and ultimate tensile strength is increasing, while ductility is decreasing with increasing mean stress and stress amplitude.

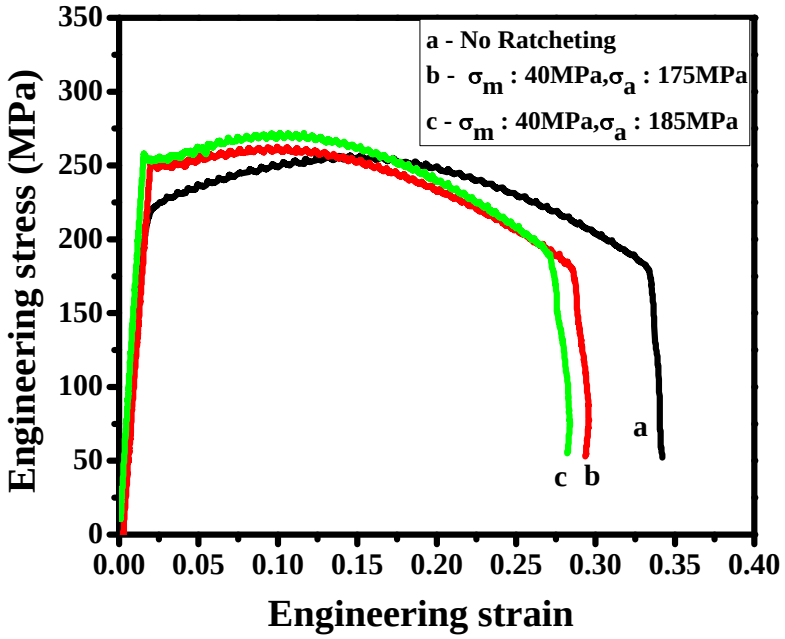

Fig. 4.21: Variation of post-fatigue tensile properties in annealed condition for varying σ_a (175, 185 MPa) at constant σ_m : 40 MPa.

Figure 4.22 illustrate the effect of σ_a (175, 185 MPa) on post-fatigue tensile properties at constant σ_m= 45 MPa respectively. Similar results have been re-examined in this case.

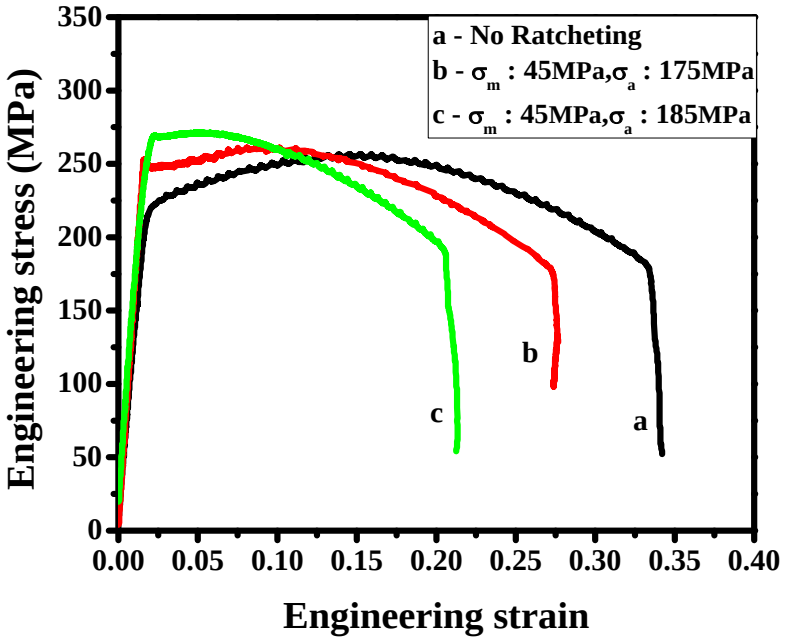

Fig. 4.22: Variation of post-fatigue tensile properties in annealed condition for varying σ_a (175, 185 MPa) at constant σ_m : 45 MPa.

Figure 4.23 and Figure 4.24 illustrate the variation in post-fatigue tensile properties in normalised condition. Similar trend has been observed at all σ_m level of 30, 35, 40 MPa. This shows material is getting cyclically hardened with increasing σ_m and σ_a.

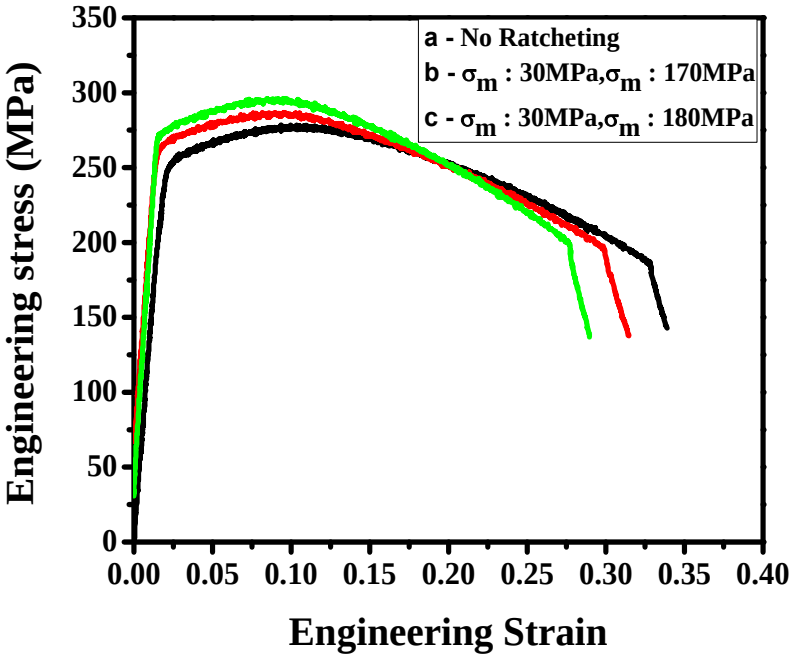

Fig. 4.23: Variation of post-fatigue tensile properties in normalised condition for varying σ_a (170, 180 MPa) at constant σ_m : 30 MPa.

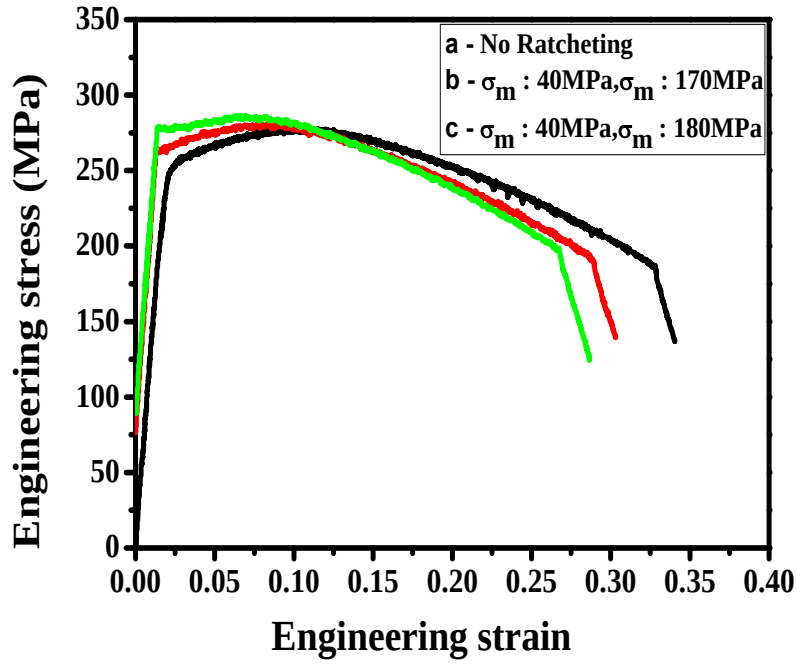

Fig. 4.24: Variation of post-fatigue tensile properties in normalised condition for varying σ_a (170, 180 MPa) at constant σ_m : 40 MPa.

4.5.5 Post-fatigue tensile properties: Effect of mean stress at constant stress amplitude

When mean stress is varied at constant stress amplitude similar results have been found as discussed in the previous section. Figure 4.25 and Figure 4.26 presents the variation in post-fatigue tensile properties for varying σ_m (40, 45 MPa) at constant σ_a level of 170 and 180 MPa in annealed condition respectively. Values of yield strength, ultimate tensile strength and total elongation percentage are tabulated in Table 4.3. From these table it is clear that strength of the material is increasing with σ_m at constant σ_a = 185 MPa.

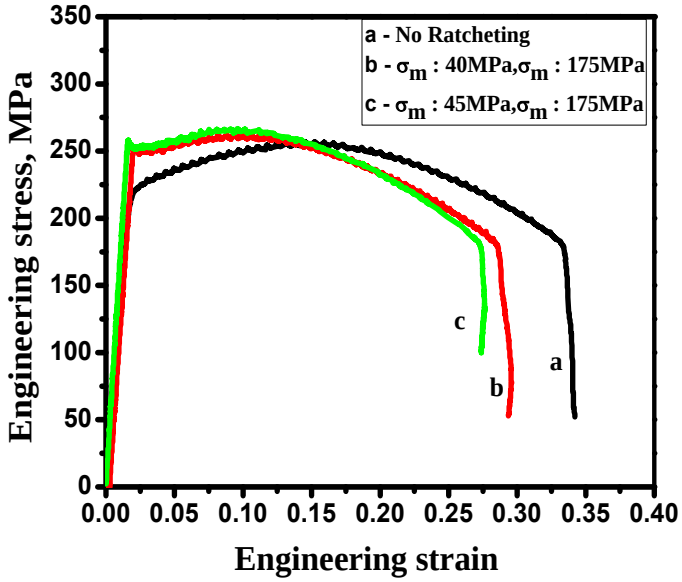

Fig. 4.25: Variation of post-fatigue tensile properties in annealed condition for varying σ_m (40, 45MPa) at constant σ_a : 175 MPa.

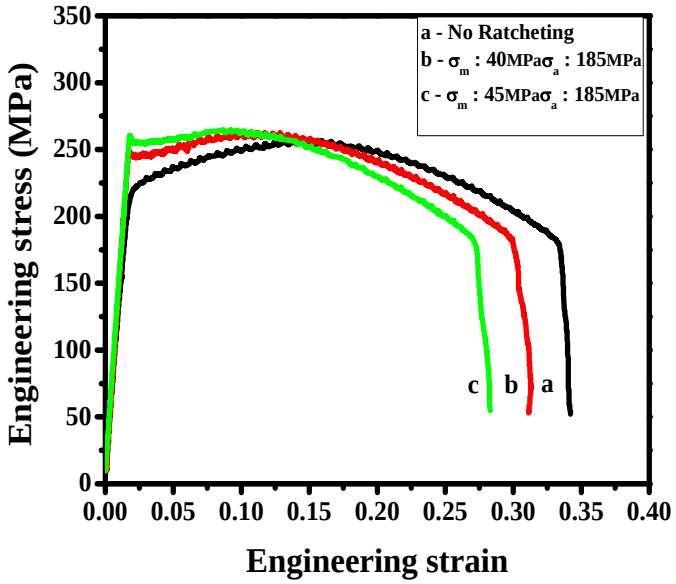

Fig. 4.26: Variation of post-fatigue tensile properties in annealed condition for varying σ_m (40, 45MPa) at constant σ_a : 185 MPa.

Table 4.4: Variation in post-fatigue tensile properties in annealed condition at constant σ_m : 45MPa

Loading Condition	Yield Strength	Ultimate Tensile Strength	Total Elongation %
No Ratcheting	221	256	34.20
σ_m : 45MPa, σ_a: 175MPa	249	261	27.66
σ_m : 45MPa, σ_a: 185MPa	268	271	21.34

In normalised condition the variation in post-fatigue tensile properties for varying σ_m (30, 35, 40 MPa) at constant σ_a level of 170 and 180 MPa is given by Figure 4.27 and Figure 4.28. Similar results have been observed as annealed condition.

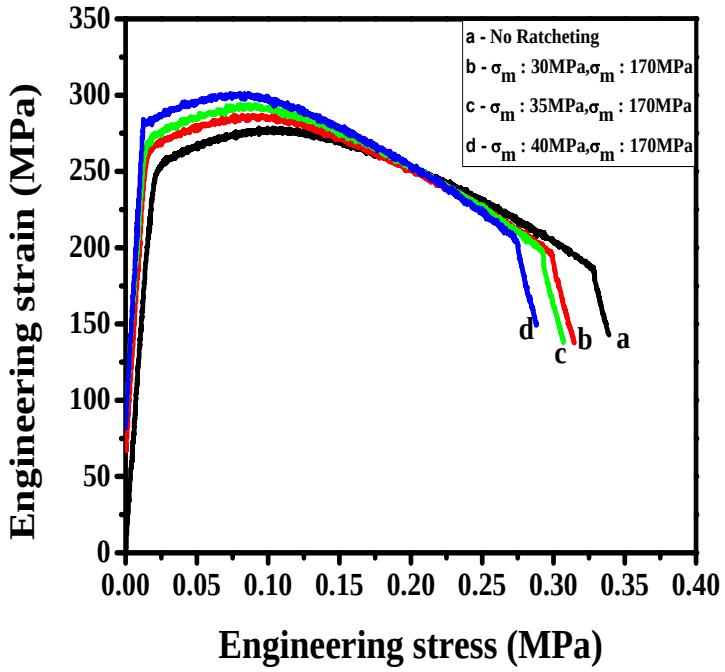

Fig. 4.27: Variation of post-fatigue tensile properties in normalised condition for varying σ_m (30, 35, 40 MPa) at constant σ_a : 170 MPa.

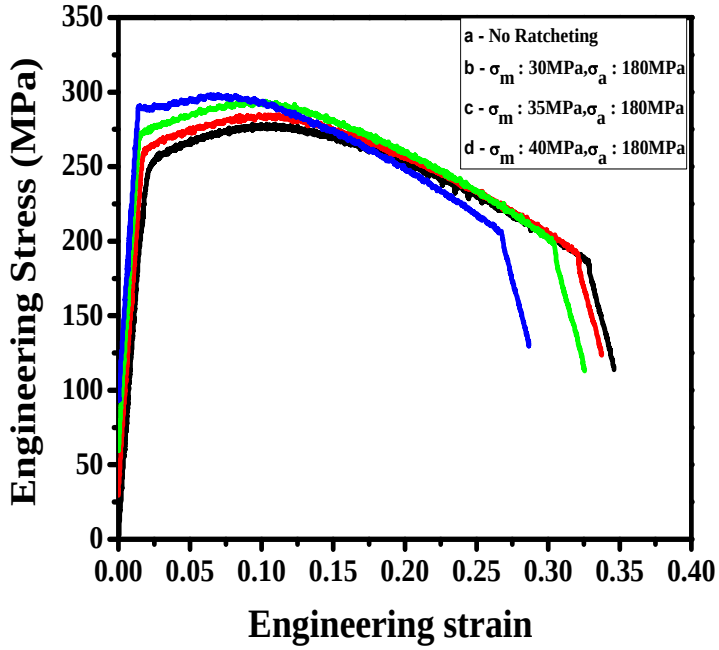

Fig. 4.28: Variation of post-fatigue tensile properties in normalised condition for varying σ_m (30, 35, 40 MPa) at constant σ_a : 180 MPa.

4.6Fractographic Observation

4.6.1 In annealed condition

After post-fatigue tensile test fracture surface of specimens were examined by scanning electron microscope (SEM). All the fractographs reveal dimpled morphology, as can be expected for a ductile material like aluminium; although all the specimens are having distinct signatures of precious cyclic loading on their morphologies. It was observed in the annealed samples that the dimple sizes vary based on their previous cyclic loading parameters. The dimple sizes decrease with increasing σ_m at constant σ_a. This is illustrated in Figure 4.29. Dimple size is estimated by using linear intercept method according to ASTM standard E112 [46]. Dimple size for varying σ_m (40, 45 MPa) at constant σ_a level of 175 and 185 MPa is tabulated in Table 4.5 and 4.6. Dimple size is decreasing with increasing σ_m and σ_a. This fact may be correlated with the decrease in grain size and increase in strength, as is described by

the Hall-Petch relationship [1]. In this case also, the strength is increasing with increasing strain accumulation during ratcheting.

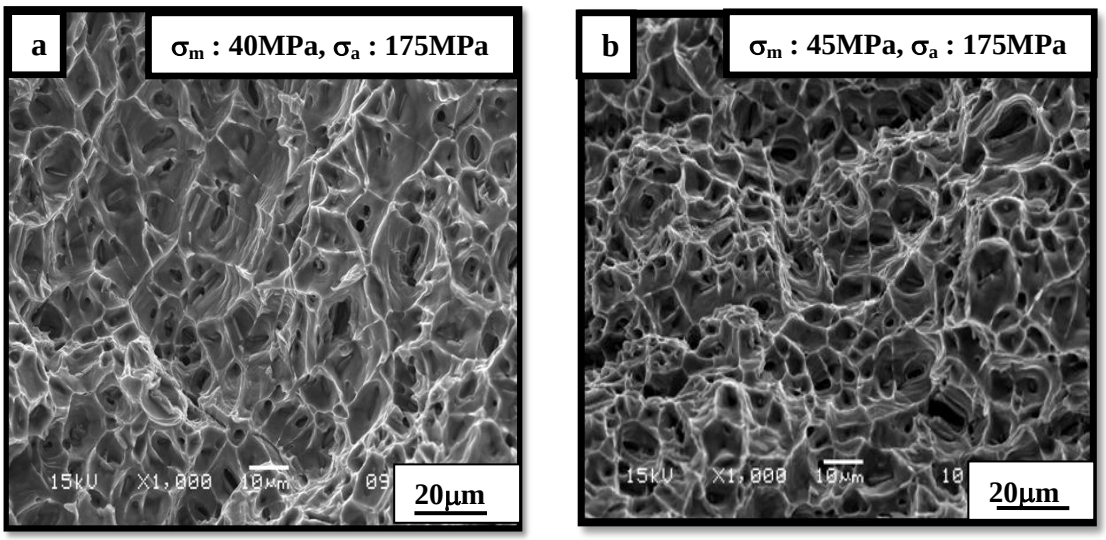

Fig. 4.29: Fracture surface of fatigue specimen (a) σ_m : 40 MPa, σ_a : 175 MPa (b) σ_m : 45 MPa, σ_a : 175MPa.

At constant stress amplitude

Table 4.5: Variation in dimple size at constant σ_a : 175MPa

Loading Condition	Dimple Size(μm)
σ_m : 40 MPa, σ_a : 175 MPa	8.53
σ_m : 45 MPa, σ_a : 175MPa	6.99

Table 4.6: Variation in dimple size at constant σ_a : 185MPa

Loading Condition	Dimple Size(μm)
σ_m : 40 MPa, σ_a : 185 MPa	6.65
σ_m : 45 MPa, σ_a : 185 MPa	6.25

4.6.2 In normalised condition

Figure 4.30 shows the images of the fracture surfaces of post-fatigue tensile specimen (in normalised condition) for different combination of σ_a and σ_m. .From these images it is clear that dimple size is decreasing with increasing σ_a .Variation in dimple size at constant σ_m = 30 MPa is tabulated in Table 4.7. Table 4.8 shows the variation in dimple size at constant σ_a = 170 MPa. To determine the secondary phase EDS analysis is done. Figure 4.31 shows the EDS spectra of σ_m = 30MPa, σ_a = 170MPa and σ_m= 40 MPa, σ_a = 180 MPa respectively.

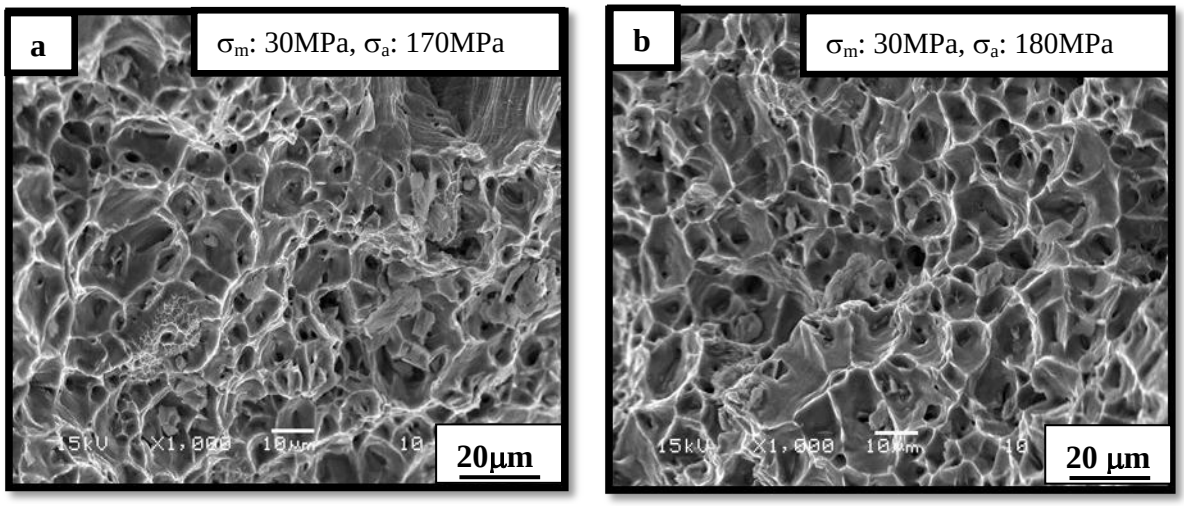

Fig.4.30: Fracture surface of fatigue specimen (a) σ_m : 30 MPa, σ_a : 170 MPa (b) σ_m : 40 MPa, σ_a : 180 MPa

Table 4.7: Variation in dimple size at constant σ_m : 30 MPa

Loading Condition	Dimple Size(μm)
σ_m : 30MPa, σ_a : 170MPa	6.28
σ_m : 30MPa, σ_a : 180MPa	5.89

Table 4.8: Variation in dimple size at constant σ_a : 170 MPa

Loading Condition	Dimple Size(μm)
σ_m : 30 MPa, σ_a : 170 MPa	6.28
σ_m : 35 MPa, σ_a: 170 MPa	5.49
σ_m : 40 MPa, σ_a: 170 MPa	5.41

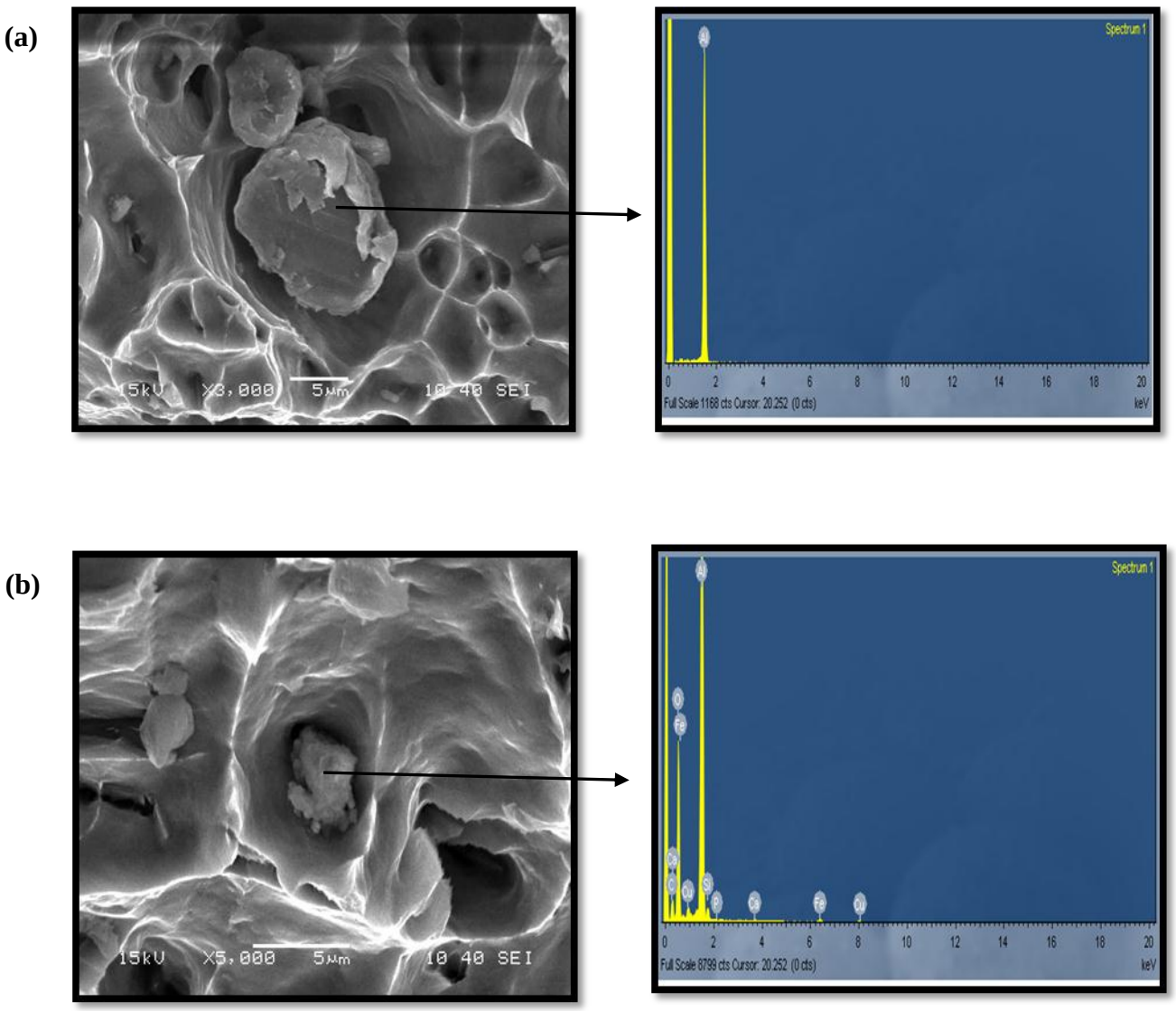

Fig. 4.32: EDS spectra (a) σ_m : 30 MPa, σ_a : 170 MPa (b) σ_m : 40MPa, σ_a : 180 MPa.

4.7 Hardness variation in post fatigue tensile specimen

Increase in hardness is achieved in annealed conditions after the post-fatigue tensile test with increasing σ_m and σ_a. This increment in hardness is attributed to the observed increase in strain accumulation in the specimens. Increased strain accumulation in turn causes cyclic hardening of the materials. The results of hardness tests are tabulated in Table 4.9 and 4.10 at constant σ_a level of 175, 185MPa respectively.

Table 4.9: Variation in hardness at constant σ_a : 185MPa with varying σ_m

Loading Condition	Vickers Hardness(HV_3)
σ_m : 40 MPa, σ_a : 185 MPa	95.56
σ_m : 45MPa, σ_a : 185MPa	96.95

Table 4.10: Variation in hardness at constant σ_a : 175MPa with varying σ_m

Loading Condition	Vickers Hardness(HV_3)
σ_m : 40 MPa, σ_a : 175 MPa	94.3
σ_m : 45 MPa, σ_a : 175 MPa	96.33

CHAPTER - 5

CONCLUSIONS

&

FUTURE WORK

5.0 Conclusions

The conclusions drawn from the conducted experiments are as follows:

1. Accumulation of ratcheting strain increases with increasing stress amplitude at constant level of mean stress. This fact occurs due to increase in dislocation density with increased damage of the material. Increase in dislocation density can be explained due to shifting of hysteresis loops.
2. Increase in strain accumulation with increasing mean stress at constant level of stress amplitude is also achieved due to increase of dislocation density and in this condition hysteresis loop is shifting in more stress direction strain accumulation for normalising is less compare to annealing.
3. Saturation in strain accumulation is achieved after few cycles due to attainment of stable dislocation configuration after initial 30-40 cycles. In normalising, saturation is achieved more quickly as compared to annealing. This occurs due to the fact that the dislocations find a barrier more quickly in normalised samples as the grain size is lower.
4. Post-fatigue yield strength and tensile strength increase with increasing accumulation of ratcheting strain. The fractographic features also carries this signature
5. Post-fatigue hardness of the annealed samples increases with increased accumulation of ratcheting strain. Cyclic hardening may be responsible for this phenomenon.

5.1 Scope for Future Work

The present work leaves a wide scope for future investigation:

1. In the present investigation mechanical properties of commercial pure aluminium have been studied. To study the micro-mechanism and dislocation sub-structure formation, TEM analysis should be done. During this investigation, TEM experiments could not be done.
2. The present set of tests has been done on commercially pure aluminium to understand the ratcheting phenomenon on aluminium. However, there is enough scope of work on various aluminium alloys. It may be interpreted from the current investigation that ratcheting behaviour of different aluminium alloys will be entirely different. Hence, work is needed to carry out in that direction.

CHAPTER - 6

REFERENCES

6.0 References

1. Dieter G.E., “Mechanical Metallurgy”, McGraw-Hill Book Company, 1988.
2. Paul S.K., Sivaprasad S., Dhar S., Tarafder S., “Cyclic plastic deformation and cyclic hardening/softening behaviour in 304LN stainless steel”, Theoretical and Applied Fracture Mechanics, 54 (2010): pp. 63-70.
3. Jiang Y., Sehitoglu H., “Cyclic ratcheting of 1070 steel under multiaxial stress states”, International Journal of Plasticity, 10 (1994): pp. 579-608.
4. Kang G.Z., Li Y.G., Zhang J., Sun Y.F., Gao Q., “Uniaxial ratcheting and failure behaviours of two steels”, Theoretical and Applied Fracture Mechanics, 43 (2005): pp. 199-209.
5. Gupta C., Chakravartty J.K., Reddy G.R., Banerjee S., “Uniaxial cyclic deformation behaviour of SA 333 Gr 6 piping steel at room temperature”, International Journal of Pressure Vessels and Piping, 82 (2005): pp. 459-469.
6. Ruggles M.D., Krempl E., “The interaction of cyclic hardening and ratcheting for AISI type 304 stainless steel at room temperature. I. experiments”, Journal of Mechanics and Physics of Solids, 38 (1990): pp. 575-585.
7. Zhang J., Jiang Y., “An experimental investigation on cyclic plastic deformation and substructures of polycrystalline copper, International Journal of Plasticity, 21 (2005): pp. 2191-2211.
8. Feaugas X., Gaudin C., “Ratchetting process in the stainless steel AISI 316L at 300 K: an experimental investigation”, International Journal of Plasticity, 20 (2004): pp. 643–662.
9. Hassan T., Kyriakides S., “Ratcheting of cyclically hardening and softening materials: I. uniaxial behaviour”, International Journal of Plasticity, 10 (1994): pp. 149-184.
10. Doong S.H., Socie D.F., Robertson I.M., “Dislocation substructures and non proportional hardening”, Journal of Engineering Materials and Technology, 112 (1990): pp. 456-464.
11. Mizuno M., Mima Y., Abdel-Karim M., “Uniaxial ratcheting of 316 FR Steel at room temperature - part 1: Experiments [J], ASME Journal of Engineering Materials and Technology, 122 (2000): pp. 29–34.
12. Kang G., Gao Q., “Uniaxial and non-proportionally multiaxial ratcheting of U71Mn rail steel: experiments and simulations”, Mechanics of Materials, 34 (2002): pp. 809–820.

13. Krempl E., Lu H., “The hardening and rate dependent behaviour of fully annealed type 304 stainless steel under bi-axial in-phase and out-of-phase strain cycling at room temperature”, ASME Journal of Engineering Materials and Technology, 106 (1984): pp.376-382.
14. Tasnim H., Stelios K., “Ratcheting of cyclically hardening and softening materials: I. uniaxial behaviour”, International Journal of Plasticity, 10 (1994): pp. 149–84.
15. Morrow J. D., “Cyclic plastic strain energy and fatigue of metals, in internal friction, damping and cyclic plasticity, ASTM STP 378, American Society for Testing and Materials, Philadelphia, PA, (1965): pp. 45-84.
16. Lefebvre D., Ellyin F., “Cyclic response and inelastic strain energy in low cycle fatigue”, International Journal of Fatigue, 6 (1984): pp. 9-15.
17. Ellyin F., “Fatigue damage, crack growth and life prediction”, Chapman and Hall, (1997).
18. Kujawski D. , Kallianpur V., Krempl E., “An experimental study of uniaxial creep, cyclic creep and relaxation of AISI type 304 stainless steel at room temperature”, Journal of the Mechanics and Physics of Solids, 28 (1980): pp. 129-148.
19. Gaudin C., Feaugas X., “Cyclic creep process in AISI 316L stainless steel in terms of dislocation patterns and internal stresses”, Acta Materialia, 52 (2004): pp. 3097-3110.
20. Satyadevi A., Sivakumar S.M., Bhattacharya S.S., “A new failure criterion for materials exhibiting ratcheting during very low cycle fatigue”, Materials Science and Engineering A, 452 (2007): pp. 380-385.
21. Paul S.K., Sivaprasad S., Dhar S., Tarafder S., “True stress control asymmetric cyclic plastic behaviour in SA333 C-Mn steel”, International Journal of Pressure Vessel and Piping, 87 (2010): pp. 440-446.
22. Chen G., Chen X., Niu C-D, “Uniaxial ratcheting behaviour of 63Sn37Pb solder with loading histories and stress rates”, Materials Science and Engineering A, 421 (2010): pp. 238-244.
23. Ray K.K., Dutta K., Shivprasad S., Tarafdar S., “Fatigue damage of AISI304 stainless steel: role of mean stress”, Proceedia Engineering, 2 (2010): pp. 1805-1813.
24. Yang X., “Low cycle fatigue and cyclic stress ratcheting failure behaviour of carbon steel 45 under uniaxial cyclic loading”, International Journal of Fatigue, 27 (2005): pp. 1124–1132.

25. Lam P.C., Srivatsan T.S., Hotton B., Al-Hajri M., “Cyclic stress response characteristics of an aluminum–magnesium–silicon alloy”, Materials Letters, 45 (2000): pp. 186-190.
26. Lim C-B., Kim K.S., Seong J.B., “Ratcheting and fatigue behaviour of a copper alloy under uniaxial cyclic loading with mean stress”, International Journal of Fatigue, 31 (2009): pp. 501-507.
27. Zhang X.P., Castagne S., Gu C.F., Luo X.F., “Effects of annealing treatment on the ratcheting behaviour of extruded AZ31B magnesium alloy under asymmetrical uniaxial cyclic loading”, Journal of Materials Science, 46 (2011): pp. 1124-1131.
28. Mcdowell D.L., “Stress rate dependence of cyclic ratcheting behaviour of two rail steels”, International Journal of Plasticity, 14 (1998): pp. 355-390.
29. Xia Z., Kujawski D., Ellyin F., “Effect of mean stress and ratcheting strain on fatigue life of steel”, International Journal of Fatigue, 96 (1995): pp. 335-341.
30. Mercer M.E., Dickerson S.L., Gibeling J.C., “Cyclic deformation of dispersion strengthened aluminium alloys”, Materials Science and Engineering A, 203 (1995): pp. 46-58.
31. Chen G., Shan S-C., Chen X., Yuan H., “Ratcheting and fatigue properties of the high-nitrogen steel X13CrMnMoN18-14-3 under cyclic loading”, Computational Materials Science, 46 (2010): pp. 572–578.
32. Tikhovski I., Molders M., Wiemann M., Bingmann D., Fischer A., “Fatigue behaviour and in-vitro biocompatibility of the Ni-free austenitic high-nitrogen steel X13CrMnMoN18-14-3”, ASTM Committee F04 on Medical and Surgical Materials and Devices, 1438 (2002): pp. 119-136
33. Feltner C.E., Laird C., “Cyclic stress strain response of F.C.C. metals and alloys. I. phenomenological experiments and II. dislocation structure and mechanisms”, Acta Metallurgica, 15 (1967): pp. 1621-1653.
34. Kang G., Liu Y., Dong Y., Gao Q., “Uniaxial ratcheting behaviours of metals with different crystal structures or values of fault energy: macroscopic experiments”, Materials Science and Technology, (2010): Accepted.
35. Pickard A.C., Knott J.F., “Effect of testing method on cyclic hardening behaviour in face-centered-cubic alloys, in low cycle fatigue, American Society for Testing and Materials, Philadelphia, PA, (1988): pp. 58-76.

36. Wang Q.G., Apelian D., Lados D.A., “Fatigue behaviour of A356-T6 aluminum cast alloys. Part I. effect of casting defects”, Journal of Light Metals, 1 (2001): pp. 73–84.
37. Bari S., Hassan T., “Anatomy of coupled constitutive model for ratcheting simulation”, International Journal of Plasticity, 16 (2000): pp. 381-409.
38. Bari S., Hassan T., “Kinematic hardening rules in uncoupled modelling for multiaxial ratcheting simulation”, International Journal of Plasticity, 17 (2001): pp. 885-905.
39. Chaboche J.L., Nouaihas D., “Constitutive modelling of ratcheting effects. part I experimental facts and properties of classical models”, ASME Journals of Engineering Materials and Technology, 3 (1989): pp. 384-390.
40. Armstrong P.J., Frederick C.O., “A mathematical representation of multiaxial Bauschinger effect”, Technical Report RD/B/N731, Berkeley Nuclear Laboratories, (1966).
41. Prager W., “A new method of analyzing stress and strain in work hardening plastic solids”, Journal of Applied Mechanics, 23 (1956): pp. 493-496.
42. Ohno N., Wang J.D., “Kinematic hardening rules with critical state of dynamic recovery, part II applications to experiments of ratcheting behaviour”, International Journal of Plasticity, 9 (1993): pp. 391-403.
43. Wallin M., Ristinmaa M., Ottosen N.S., “Kinematic hardening in large strain plasticity”, European Journal of Mechanics – A/Solids, 22 (2003): pp. 341-356.
44. Suresh S., Fatigue of Materials, Cambridge University Press, (1996).
45. Dogui A., Sidoroff F., “Kinematic hardening in large elstoplastic strain”, Engineering Fracture Mechanics, 21 (1985): pp. 685-695.
46. E112, “Standard test methods for determining grain size”, Annual book of ASTM standards, West Conshohocken, PA, 2003.
47. E606, “Standard practice for Strain Controlled Fatigue Testing, Annual Book of ASTM Standards, West Conshohocken, PA, 1998.
48. Kang G., Ding J., Liu Y., “Summary on uniaxial ratchetting of 6061-T6 aluminium alloy”, Aluminium Alloys, Theory and Applications, pp. 199-216.